Author/s:
Koutsakos, M;Rowntree, LC;Hensen, L;Chua, BY;van de Sandt, CE;Habel, JR;Zhang, W;Jia, X;Kedzierski, L;Ashhurst, TM;Putri, GH;Marsh-Wakefield, F;Read, MN;Edwards, DN;Clemens, EB;Wong, CY;Mordant, FL;Juno, JA;Amanat, F;Audsley, J;Holmes, NE;Gordon, CL;Smibert, OC;Trubiano, JA;Hughes, CM;Catton, M;Denholm, JT;Tong, SYC;Doolan, DL;Kotsimbos, TC;Jackson, DC;Krammer, F;Godfrey, DI;Chung, AW;King, NJC;Lewin, SR;Wheatley, AK;Kent, SJ;Subbarao, K;McMahon, J;Thevarajan, I;Nguyen, THO;Cheng, AC;Kedzierska, K

Title:
Integrated immune dynamics define correlates of COVID-19 severity and antibody responses

Date:
2021-03-16

Citation:
Koutsakos, M., Rowntree, L. C., Hensen, L., Chua, B. Y., van de Sandt, C. E., Habel, J. R., Zhang, W., Jia, X., Kedzierski, L., Ashhurst, T. M., Putri, G. H., Marsh-Wakefield, F., Read, M. N., Edwards, D. N., Clemens, E. B., Wong, C. Y., Mordant, F. L., Juno, J. A., Amanat, F. ,... Kedzierska, K. (2021). Integrated immune dynamics define correlates of COVID-19 severity and antibody responses. Cell Reports Medicine, 2 (3), https://doi.org/10.1016/j.xcrm.2021.100208.

Persistent Link:
https://hdl.handle.net/11343/272883

Cell Reports
Medicine

Article

Integrated immune dynamics define correlates of COVID-19 severity and antibody responses

Graphical Abstract

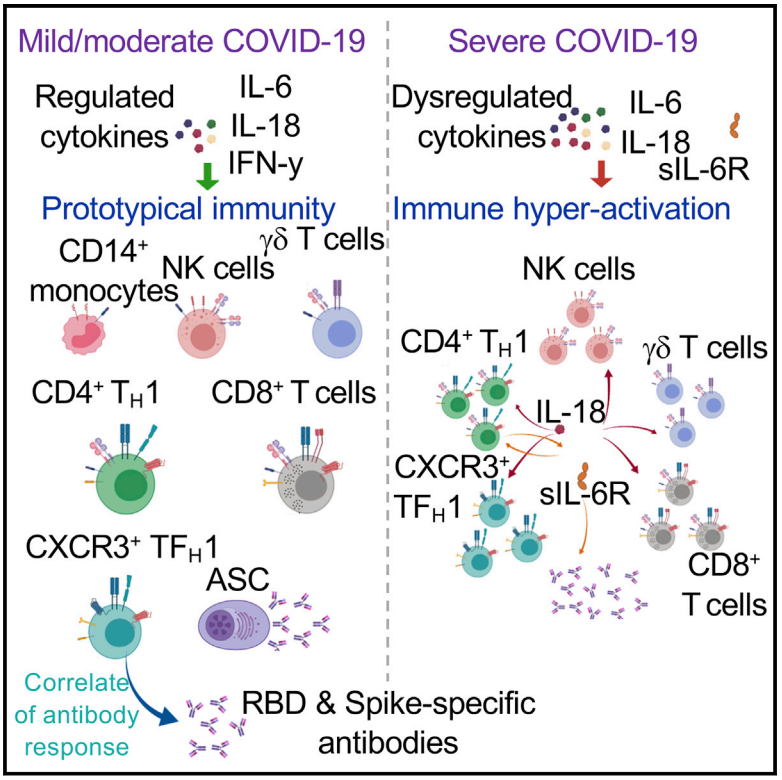

Highlights

- Analyses of 184 immune features define kinetics of immune responses to SARS-CoV-2
- Circulating $T_{FH}1$ cells in acute COVID-19 correlate with antibodies
- sIL-6R levels are elevated in severe COVID-19 but do not correlate with IL-6
- Elevated IL-6 and IL-18 correlate with immune cell hyperactivation

Authors

Marios Koutsakos, Louise C. Rowntree, Luca Hensen, ..., Thi H.O. Nguyen, Allen C. Cheng, Katherine Kedzierska

Correspondence

kkedz@unimelb.edu.au

In brief

Koutsakos et al. perform a broad analysis of 184 immune features using blood samples from 85 COVID-19 cases across time and severity groups. The study defines circulating $T_{FH}1$ cells as a correlate of antibody responses and sIL-6R, IL-6, and IL-18 as correlates of disease severity.

Koutsakos et al., 2021, Cell Reports Medicine 2, 100208
March 16, 2021
https://doi.org/10.1016/j.xcrm.2021.100208

CellPress

Cell Reports Medicine

CellPress
OPEN ACCESS

Article

Integrated immune dynamics define correlates of COVID-19 severity and antibody responses

Marios Koutsakos,[1,38] Louise C. Rowntree,[1,38] Luca Hensen,[1,38] Brendon Y. Chua,[1,2,38] Carolien E. van de Sandt,[1,3,38] Jennifer R. Habel,[1] Wuji Zhang,[1] Xiaoxiao Jia,[1] Lukasz Kedzierski,[1,4] Thomas M. Ashhurst,[5,6] Givanna H. Putri,[7,8] Felix Marsh-Wakefield,[7,9,10] Mark N. Read,[7,8,11] Davis N. Edwards,[8,11] E. Bridie Clemens,[1] Chinn Yi Wong,[1] Francesca L. Mordant,[1] Jennifer A. Juno,[1] Fatima Amanat,[12,13] Jennifer Audsley,[14]

(Author list continued on next page)

[1]Department of Microbiology and Immunology, University of Melbourne at the Peter Doherty Institute for Infection and Immunity, Melbourne, VIC, Australia
[2]Global Station for Zoonosis Control, Global Institution for Collaborative Research and Education (GI-CoRE), Hokkaido University, Sapporo, Japan
[3]Department of Hematopoiesis, Sanquin Research and Landsteiner Laboratory, Amsterdam UMC, University of Amsterdam, Amsterdam, the Netherlands
[4]Faculty of Veterinary and Agricultural Sciences, University of Melbourne, Melbourne, VIC, Australia
[5]Sydney Cytometry Core Research Facility, Charles Perkins Centre, Centenary Institute and University of Sydney, Sydney, NSW, Australia
[6]Marie Bashir Institute for Infectious Diseases and Biosecurity, University of Sydney, Sydney, NSW, Australia
[7]Charles Perkins Centre, University of Sydney, Sydney, NSW, Australia

(Affiliations continued on next page)

SUMMARY

SARS-CoV-2 causes a spectrum of COVID-19 disease, the immunological basis of which remains ill defined. We analyzed 85 SARS-CoV-2-infected individuals at acute and/or convalescent time points, up to 102 days after symptom onset, quantifying 184 immunological parameters. Acute COVID-19 presented with high levels of IL-6, IL-18, and IL-10 and broad activation marked by the upregulation of CD38 on innate and adaptive lymphocytes and myeloid cells. Importantly, activated CXCR3$^+$cT$_{FH}$1 cells in acute COVID-19 significantly correlate with and predict antibody levels and their avidity at convalescence as well as acute neutralization activity. Strikingly, intensive care unit (ICU) patients with severe COVID-19 display higher levels of soluble IL-6, IL-6R, and IL-18, and hyperactivation of innate, adaptive, and myeloid compartments than patients with moderate disease. Our analyses provide a comprehensive map of longitudinal immunological responses in COVID-19 patients and integrate key cellular pathways of complex immune networks underpinning severe COVID-19, providing important insights into potential biomarkers and immunotherapies.

INTRODUCTION

The severe acute respiratory syndrome coronavirus 2 (SARS-CoV-2) pandemic has caused >101 million infections and 2.18 million deaths worldwide (as of January 28, 2021). Infection with SARS-CoV-2 results in a spectrum of clinical presentations, called coronavirus disease 2019 (COVID-19), ranging from asymptomatic to fatal disease. Disease severity has been associated with risk factors, including age, gender, and preexisting comorbidities,[1,2] that correlate with immune responses during acute infection. While robust, broad, and transient immune responses precede patients' recovery in non-severe cases,[3–6] severe COVID-19 can be associated with exuberant cytokine responses, hyperactivation of innate immune cells and T cells,[4,6–8] and high titers of SARS-CoV-2-specific antibodies.[8] At convalescence, the majority of individuals has SARS-CoV-2-specific antibodies and B cell and T cell responses.[9–13] CD4$^+$ T cell responses appear more prominent than CD8$^+$ T cell responses in primary SARS-CoV2 infection.[13,14]

Our understanding of immune responses to SARS-CoV-2 informed the development and clinical evaluation of immunomodulatory therapies, including monoclonal antibodies that target the interleukin-6 (IL-6) signaling pathway and corticosteroids such as dexamethasone.[15] However, results from clinical trials examining the efficacies of current therapeutic approaches are inconsistent.[16] In parallel, global accelerated efforts are focused on the development of safe vaccines against SARS-CoV-2, with the main goal of eliciting neutralizing antibodies against the Spike protein.[17] Efforts are needed to understand integrated immune correlates of recovery and protection from COVID-19, and the complexity of innate and adaptive immune perturbations underpinning severe and fatal COVID-19 to inform the rational design of vaccines and identify predictors of protective immunity.

Natasha E. Holmes,[15,16,17,18] Claire L. Gordon,[1,15] Olivia C. Smibert,[15,19,20] Jason A. Trubiano,[18,19,20,21] Carly M. Hughes,[22] Mike Catton,[23] Justin T. Denholm,[14,24] Steven Y.C. Tong,[14,24,25] Denise L. Doolan,[26] Tom C. Kotsimbos,[27,28] David C. Jackson,[1,2] Florian Krammer,[12] Dale I. Godfrey,[1,29] Amy W. Chung,[1] Nicholas J.C. King,[5,6,7,9,30,31] Sharon R. Lewin,[14,24,32] Adam K. Wheatley,[1,33] Stephen J. Kent,[1,33,34] Kanta Subbarao,[1,35] James McMahon,[22,32] Irani Thevarajan,[14,24] Thi H.O. Nguyen,[1,38] Allen C. Cheng,[36,37,38] and Katherine Kedzierska[1,2,38,39,*]

[8]School of Computer Science, University of Sydney, Sydney, NSW, Australia
[9]School of Medical Sciences, Faculty of Medicine and Health, University of Sydney, Sydney, NSW, Australia
[10]Vascular Immunology Unit, Discipline of Pathology, School of Medical Sciences, University of Sydney, Sydney, NSW, Australia
[11]The Westmead Initiative, University of Sydney, Sydney, NSW, Australia
[12]Department of Microbiology, Icahn School of Medicine at Mount Sinai, New York, NY, USA
[13]Graduate School of Biomedical Sciences, Icahn School of Medicine at Mount Sinai, New York, NY 10029-6574, USA
[14]Department of Infectious Diseases, University of Melbourne at the Peter Doherty Institute for Infection and Immunity, Melbourne, VIC, Australia
[15]Department of Infectious Diseases, Austin Hospital, Heidelberg, VIC, Australia
[16]Department of Medicine and Radiology, University of Melbourne, Parkville, VIC, Australia
[17]Data Analytics Research and Evaluation (DARE) Centre, Austin Health and University of Melbourne, Heidelberg, VIC, Australia
[18]Centre for Antibiotic Allergy and Research, Department of Infectious Diseases, Austin Health, Heidelberg, VIC, Australia
[19]Department of Infectious Diseases, Peter McCallum Cancer Centre, Melbourne, VIC, Australia
[20]National Centre for Infections in Cancer, Peter McCallum Cancer Centre, Melbourne, VIC, Australia
[21]Department of Medicine (Austin Health), University of Melbourne, Heidelberg, VIC, Australia
[22]Monash Infectious Diseases, Monash Medical Centre, Monash Health, Melbourne, VIC, Australia
[23]Victorian Infectious Diseases Reference Laboratory, Royal Melbourne Hospital at the Peter Doherty Institute for Infection and Immunity, Melbourne, VIC, Australia
[24]Victorian Infectious Diseases Services, Royal Melbourne Hospital and Doherty Department University of Melbourne, at the Peter Doherty Institute for Infection and Immunity, Melbourne VIC, Australia
[25]Menzies School of Health Research, Charles Darwin University, Darwin, NT, Australia
[26]Centre for Molecular Therapeutics, Australian Institute of Tropical Health & Medicine, James Cook University, Cairns, QLD, Australia
[27]Department of Medicine, Central Clinical School, Monash University, Melbourne, VIC, Australia
[28]Department of Allergy, Immunology, and Respiratory Medicine, Alfred Hospital, Melbourne, VIC, Australia
[29]Australian Research Council Centre of Excellence for Advanced Molecular Imaging at the University of Melbourne, Melbourne, VIC, Australia
[30]Viral Immunopathology Laboratory, Discipline of Pathology, School of Medical Sciences, University of Sydney, Sydney, NSW, Australia
[31]Sydney Nano, University of Sydney, Sydney, NSW 2006, Australia
[32]Department of Infectious Diseases, Monash University and Alfred Hospital, Melbourne, VIC, Australia
[33]ARC Centre of Excellence in Convergent Bio-Nano Science and Technology, University of Melbourne, Melbourne, VIC, Australia
[34]Melbourne Sexual Health Centre, Infectious Diseases Department, Alfred Health, Central Clinical School, Monash University, Melbourne, VIC, Australia
[35]World Health Organization Collaborating Centre for Reference and Research on Influenza at the Peter Doherty Institute for Infection and Immunity, Melbourne, VIC, Australia
[36]School of Public Health and Preventive Medicine, Monash University, Melbourne, VIC, Australia
[37]Infection Prevention and Healthcare Epidemiology Unit, Alfred Health, Melbourne, VIC, Australia
[38]These authors contributed equally
[39]Lead contact
*Correspondence: kkedz@unimelb.edu.au
https://doi.org/10.1016/j.xcrm.2021.100208

We performed in-depth analyses of broad innate and adaptive immune responses in longitudinal acute and convalescent blood samples from SARS-CoV-2-infected individuals. Our study revealed integrated innate and adaptive immune dynamics during COVID-19 up to 102 days post-disease symptom onset, with circulating T follicular helper (cT_{FH}) cells strongly correlating with levels of SARS-CoV-2-specific antibodies. We identified IL-18, soluble IL-6 receptor (sIL-6R), and hyperactivated immune responses depicted with high CD38 expression ($CD4^+$, $CD8^+$, $\gamma\delta$ T cells, innate cells) and human leukocyte antigen-DR isotype (HLA-DR) expression (natural killer [NK] cells) as correlates of COVID-19 severity, as well as correlations between dysregulation of cytokines and immune hyperactivation, providing important insights into potential biomarkers and immunotherapies.

RESULTS

COVID-19 cohort study design

We recruited 85 PCR-confirmed COVID-19 cases. A total of 33 symptomatic/hospitalized individuals were recruited, including 20 ward patients (4 requiring supplemental oxygen support), 12 intensive care unit (ICU) patients (8 requiring invasive ventilation, 3 requiring non-invasive oxygen support), and 1 outpatient. Twenty-three donors were longitudinally sampled up to 6 times while in the hospital and 13 of the donors were sampled into convalescence, between days 20 and 80 post-symptom onset. An additional 52 COVID-19-recovered individuals were recruited after discharge from the hospital (n = 9) or after recovering at home (n = 43) (Figure 1A; Tables S1 and S2), with 4 being longitudinally sampled twice between days 26 and 102 post-

CellPress
OPEN ACCESS

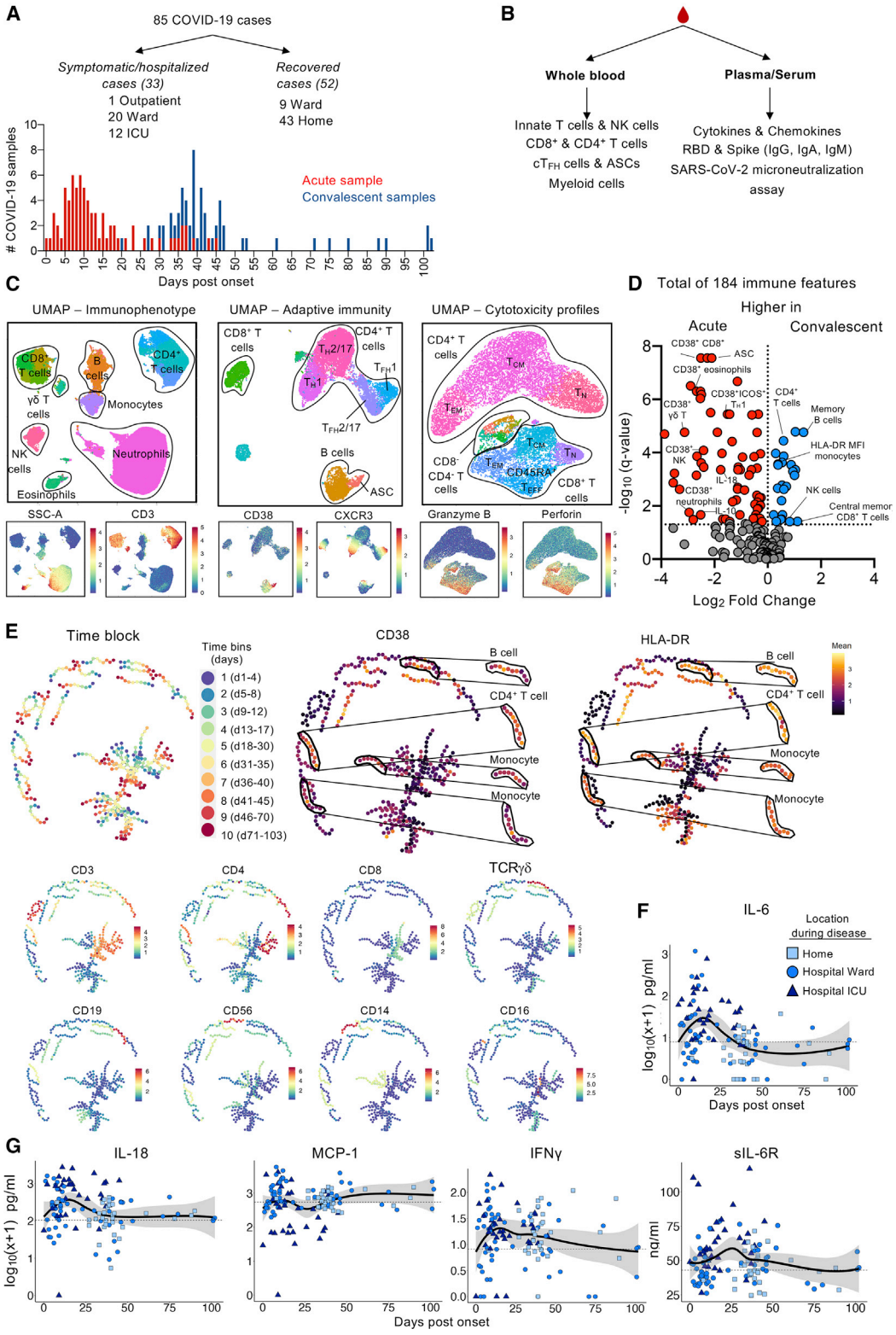

(legend on next page)

symptom onset for immune profiling and serological analyses (Figure 1B). Acute samples were obtained either during the hospital stay in hospitalized patients or within 2 weeks post-symptom onset for the non-hospitalized individuals (outpatient) (Figure 1A, in red). Convalescent samples were obtained either after hospital discharge or at the earliest day 26 post-symptom onset for non-hospitalized individuals (Figure 1A, in blue). Disease severity was determined according to whether the patients recovered at home (mild disease), the hospital ward (moderate disease), or the ICU (severe disease). A total of 66 healthy individuals and 11 non-COVID-19 hospitalized patients were assessed as controls. Our study included 1 ICU patient, no. 1-088, with a hematological malignancy treated with rituximab medication, thus lacking B cells. As this donor had no detectable SARS-CoV-2 antibodies, only cellular and cytokine data were included in the statistical analyses.

Breadth of innate, adaptive, and myeloid immune responses in COVID-19

To understand the dynamics of immune responses to SARS-CoV-2 over time, we analyzed blood from acute and convalescent individuals using 3 multi-parameter flow cytometric panels. The acute group included moderate (ward) and severe (ICU) samples. Using a computational pipeline in the Spectre R package, encompassing the FlowSOM and UMAP (uniform manifold approximation and projection) algorithms,[18] we identified clusters representing major lymphocyte and myeloid lineages and their activation phenotype from the first panel, clusters of adaptive B cell and T cell subsets from the second panel, and cytotoxicity profiles of $CD8^+$ and $CD4^+$ T cells from the third panel (Figure 1C). The UMAP analysis revealed different subsets of B helper and T_H cells according to CD38 and CXCR3, respectively (second panel), and preferentially high expression of granzyme B and perforin on $CD8^+$ effector memory (T_{EM}) and effector memory $CD45RA^+$ (T_{EMRA}) T cell subsets (third panel) (Figure 1C). To assess immune profiles between acute and convalescent COVID-19 samples, we combined our FlowSOM clustered data with the data from 14 soluble mediators and plasma receptor binding domain (RBD)-specific immunoglobulin G (IgG), IgM, and IgA antibodies to generate a total of 184 immune features. During acute COVID-19 in hospitalized patients, we observed significant changes in immune compositions compared to healthy controls and/or convalescent samples, particularly a greater proportion of neutrophils, neutrophil-to-lymphocyte and neutrophil-to-T cell ratios, higher proportions of activated populations of $CD38^+$ neutrophils, $CD38^+$ eosinophils, CD38 expression on $CD14^+$ and $CD16^+$ monocytes, $CD38^+CD56^{dim}$ NK cells, $CD38^+\gamma\delta$ T cells, antibody-secreting cells (ASCs), $PD\text{-}1^+ICOS^+$ cT_{FH} cells, $CD38^+CD4^+$ T cells, $HLA\text{-}DR^+CD4^+$ T cells, and higher proportions of T_{EMRA}-like $CD27^-CD45RA^+$, and $CD38^+CD8^+$ T cells (Figures 1D, S1, and S2). During convalescence, we found higher proportions of T_{CM} $CD8^+$ T cells, NK cells, T_{CM}, and T_{EM} $CD4^+$ T cells (Figures 1D and S1;Table S4).

To assess immune activation over time, we implemented a time-series algorithm called TrackSOM on the first immunophenotyping panel. TrackSOM is a time series-based clustering and cluster evolution tracking algorithm that combines the single time point clustering capacity of FlowSOM with the tracking by ChronoClust[19] of cluster developments over time. TrackSOM clusters data from all time points using FlowSOM, and thus determines the temporal evolutions of the resulting metaclusters and clusters using the tracking mechanism of ChronoClust. With TrackSOM, we categorized, or "binned," samples into 10 time intervals ("bins") post-disease onset (i.e., bin 1 = 1–4, bin 2 = 5–8, bin 3 = 9–12 days, and so on) to allow for at least 4 samples (n = 4–15) per time bin (Figures 1E and S3; Table S3). Strikingly, the tracking pattern of the CD38 activation marker indicated dynamic activation of both innate and adaptive cells peaking within weeks 2–4 of disease onset (bins 4–6) before declining at later time bins (Figure 1E). These patterns were still apparent when we excluded ICU patient no. 1-088, who had continuously high CD38 expression over 4 time points. The expression of HLA-DR was also dynamic across time points, but to a lesser extent. Overall, our analyses revealed differences in immune profiles across the time between acute and convalescent phases, with broad immune activation of innate, adaptive, and myeloid cells.

Rapid and transient activation of innate immune cells during COVID-19

To define the dynamics of innate responses, we compared 14 cytokines/chemokines in moderate and severe acute and convalescent COVID-19 plasma samples over time, in comparison to healthy controls. As IL-6 is a key driver of inflammation in COVID-19, possibly mediating pathology via engaging sIL-6R on cells expressing the gp130 co-receptor,[20] we also measured sIL-6R levels, since the role of sIL-6R in COVID-19 remains unknown. Inflammatory cytokines IL-6, IL-18, and IL-10 were significantly upregulated in acute samples compared to convalescent samples (Figures 1F, 1G, and S4A), consistent with other studies.[21–23] The levels of monocyte chemoattractant protein-1 (MCP-1), interferon-γ (IFN-γ), and sIL-6R were also higher in acute samples from some patients compared to healthy controls, but these responses were variable (Figures 1G, S4A, and S4B), possibly reflecting the grouping of all ward and ICU patients in this analysis.

To complement our computational analysis, we applied manual gating (Figure S5) for immune subsets that contribute

Figure 1. Broad immune activation in longitudinal COVID-19 samples

(A and B) Overviews of (A) cohort and samples collected and (B) analyses performed.

(C) UMAP plot from FlowSOM analysis for 3 flow-cytometric panels, with representative clusters and expression profiles.

(D) Volcano plot of 184 immune features in acute and convalescent samples, with key representative features labeled.

(E) TrackSOM analysis of samples stained with the immunophenotype panel, with plots showing time bins of lineage-defining markers and the activation markers CD38 and HLA-DR. Time bins were days 1–4, 5–8, 9–12, 13–17, 18–30, 31–35, 36–39, 41–45, 46–53, and 71–102 (Table S3).

(F and G) Levels of cytokines (F) IL-6 and (G) IL-18, MCP-1, IFN-γ, and sIL-6R in COVID-19 plasma across time. Locally estimated scatterplot smoothing (LOESS) regression line and 95% confidence interval (CI) are shown, n = 119.

CellPress
OPEN ACCESS

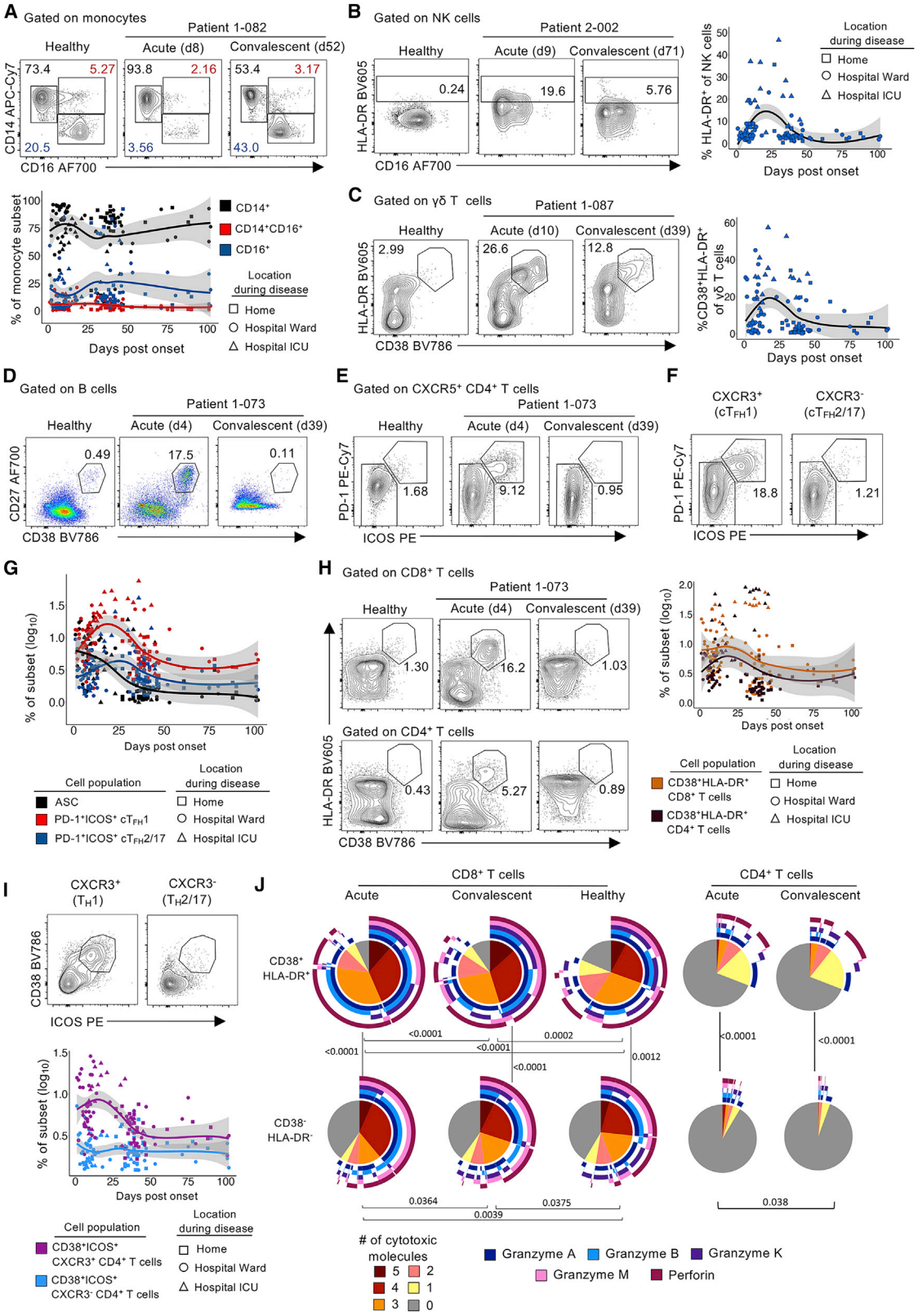

(legend on next page)

to antiviral immunity in COVID-19 and influenza.[24–27] Manual gating showed significantly higher activation of immune subsets in acute COVID-19 compared to convalescent and healthy donors (Figure S6A). For innate populations, acute samples had significantly higher proportions of activated HLA-DR$^+$ NK cells, CD38$^+$HLA-DR$^+$ γδ T cells, and effector-like CD27$^-$CD45RA$^+$ γδ T cells, but lower levels of non-classical CD16$^+$ monocytes, compared to convalescent and/or healthy donors (Figures 2A–2C; S6B, and S6C). The number of monocytes and γδ T cells were comparable between acute and convalescent samples, while NK cell numbers were significantly lower in the acute samples (Figure S6D). These highly activated innate cell populations were dynamic, peaking within the first 3–4 weeks and declining thereafter (Figures 2A–2C).

Longitudinal dynamics of B cells, cT$_{FH}$ cells, Th1 CD4$^+$, and CD8$^+$ T cells in COVID-19

We next defined immune populations that underpin the induction of humoral and cellular adaptive immunity, B cells, cT$_{FH}$ cells, Th1 CD4$^+$ cells, and CD8$^+$ T cells. We observed significantly higher proportions and numbers of CD38^{hi}CD27$^+$ ASCs and activated PD-1$^+$ICOS$^+$CXCR5$^+$CD4$^+$ cT$_{FH}$ cells (Figures 2D, 2E, and S6E), a subset of lymphoid T$_{FH}$ cells, in the blood[28] of acute COVID-19 patients compared to subsets in convalescent or healthy donors. Moreover, the activation of cT$_{FH}$ cells by the co-expression of PD-1 and ICOS was attributed more to CXCR3$^+$ cT$_{FH}$-type 1 (cT$_{FH}$1) cells than CXCR3$^-$ cT$_{FH}$2/cT$_{FH}$17 cells (Figures 2F and S6E). Proportions of ASCs increased rapidly and transiently at disease onset, while activated cT$_{FH}$1 cells gradually increased, peaking after 3–4 weeks, similar to activated innate cells, with cT$_{FH}$1 cell numbers maintained at convalescence (Figures 2G and S6E). There was substantial CD38$^+$HLA-DR$^+$ CD8$^+$ and CD4$^+$ T cell activation during the acute phase, as determined by increased proportions and numbers (Figure S6F). Both populations peaked earlier within the first 2–3 weeks and declined thereafter for home and ward patients but remained high until weeks 6–7 for ICU patients (Figure 2H). We also observed greater proportions and numbers of activated PD-1$^+$CD38$^+$ and CXCR3$^+$CD38$^+$ CD8$^+$ T cells (Figure S6F) and greater proportions of CD27$^-$CD45RA$^+$ T$_{EMRA}$-like and CD27$^-$CD45RA$^-$ T$_{EM}$-like CD8$^+$ T cells in acute samples compared to convalescent or healthy controls (Figure S5G). Similarly, greater proportions of CD27$^-$CD45RA$^-$ T$_{EM}$ CD4$^+$ T cells were detected in acute samples (Figure S6G). In line with the T$_H$1 environment of a viral infection, CXCR3$^+$ T$_H$1 cells highly expressed CD38 with ICOS, factors that were absent in CXCR3$^-$ T$_H$2/17 cells (Figures 2I and S6F).

To define cytotoxic profiles of CD8$^+$ and CD4$^+$ T cells, the expression of granzyme A, B, K, and M and perforin was assessed. Activated CD38$^+$HLA-DR$^+$ CD8$^+$ T cells in acute samples expressed higher levels of granzyme A and B and perforin compared to healthy and/or convalescent patients (Figures S7A and S7B). In addition, activated CD38$^+$HLA-DR$^+$ CD8$^+$ T cells in acute samples had higher proportions of cells expressing multiple cytotoxic molecules, with the majority of CD38$^+$HLA-DR$^+$ CD8$^+$ T cells expressing 3 or 4 cytotoxic molecules (Figure 2J). Although the expression of granzyme B and perforin within CD38$^+$HLA-DR$^+$ CD8$^+$ T cells significantly decreased at convalescence, interestingly, granzyme K and M were increased (Figures S7A and S7B). The overall diversity of cytotoxic molecule expression, measured by the different combinations of molecules simultaneously expressed per cell, also differed at convalescence as compared to acute COVID-19 and healthy individuals (Figure 2J).

While modest, activated CD38$^+$HLA-DR$^+$ CD4$^+$ T cells also expressed higher levels of granzyme B in acute samples (Figures 2J, S7C, and S7D). Similar patterns were found when the expression of granzymes and perforin were analyzed according to their T cell differentiation subsets by FlowSOM analysis (Figure S8).

Overall, SARS-CoV-2 infection induced a prototypical antiviral adaptive immune response comprising ASCs, activated cT$_{FH}$1 cells, activated T$_H$1 CD4$^+$ T cells, and highly cytotoxic CD8$^+$ T cells that emerged during acute COVID-19 and contracted during convalescence.

Seroconversion and antibody signatures during acute and convalescent COVID-19

As humoral immunity plays a key role in antiviral responses, we analyzed antibodies in acute and convalescent samples from 25 COVID-19 patients across multiple time points, by comparing RBD-specific IgG, IgM, and IgA antibodies by ELISA[9] with healthy controls (Figures 3A and S9). Antibody levels were

Figure 2. Dynamic activation of innate cells, B cells, cT$_{FH}$1 cells, T$_H$1 CD4$^+$ T cells, and CD8$^+$ T cells in COVID-19 patients

(A–C) Representative fluorescence-activated cell sorting (FACS) plots of each immune population for a healthy donor and a COVID-19 patient at acute and convalescent time points.

(A) Proportion of monocyte subsets.

(B) Proportion of activated HLA-DR$^+$ NK cells.

(C) Proportion of activated CD38$^+$HLA-DR$^+$ γδ T cells in COVID-19 samples against time.

(D–F) Representative FACS plots of ASCs (D), PD-1$^+$ICOS$^+$ cT$_{FH}$ cells (E), and CXCR3$^+$ cT$_{FH}$1 and CXCR3$^-$ cT$_{FH}$2/cT$_{FH}$17 cells for a healthy donor and a COVID-19 patient at acute and convalescent time points (D and E), an acute time point from a COVID-19 patient (F).

(G) Proportion of ASCs, PD-1$^+$ICOS$^+$ CXCR3$^+$ cT$_{FH}$1 cells, and PD-1$^+$ICOS$^+$ CXCR3$^-$ cT$_{FH}$2/cT$_{FH}$17 cells in COVID-19 samples against time.

(H) Proportion of CD38$^+$HLA-DR$^+$ CD8$^+$ and CD4$^+$ T cells in COVID-19 samples against time. Representative FACS plots of each immune population for a healthy donor and a COVID-19 patient at an acute and a convalescent time point.

(I) Proportion of CD38$^+$ICOS$^+$ CXCR3$^+$ T$_H$1 and CXCR3$^-$ T$_H$2/17 CD4$^+$ cells in COVID-19 samples against time. Representative FACS plots of each population shown for an acute time point from a COVID-19 patient.

(J) Pie charts representing average fractions of CD38$^+$HLA-DR$^+$, CD38$^-$HLA-DR$^-$ CD8$^+$, and CD4$^+$ T cells co-expressing different cytotoxic molecules (slices) and the combinations of granzymes and perforin molecules (arcs). Statistical significance ($p < 0.05$) was determined by permutation tests. Data are based on the manual gating strategy, as per Figure S3.

(A–C and G–I) LOESS regression line and 95% CI are shown, n = 105.

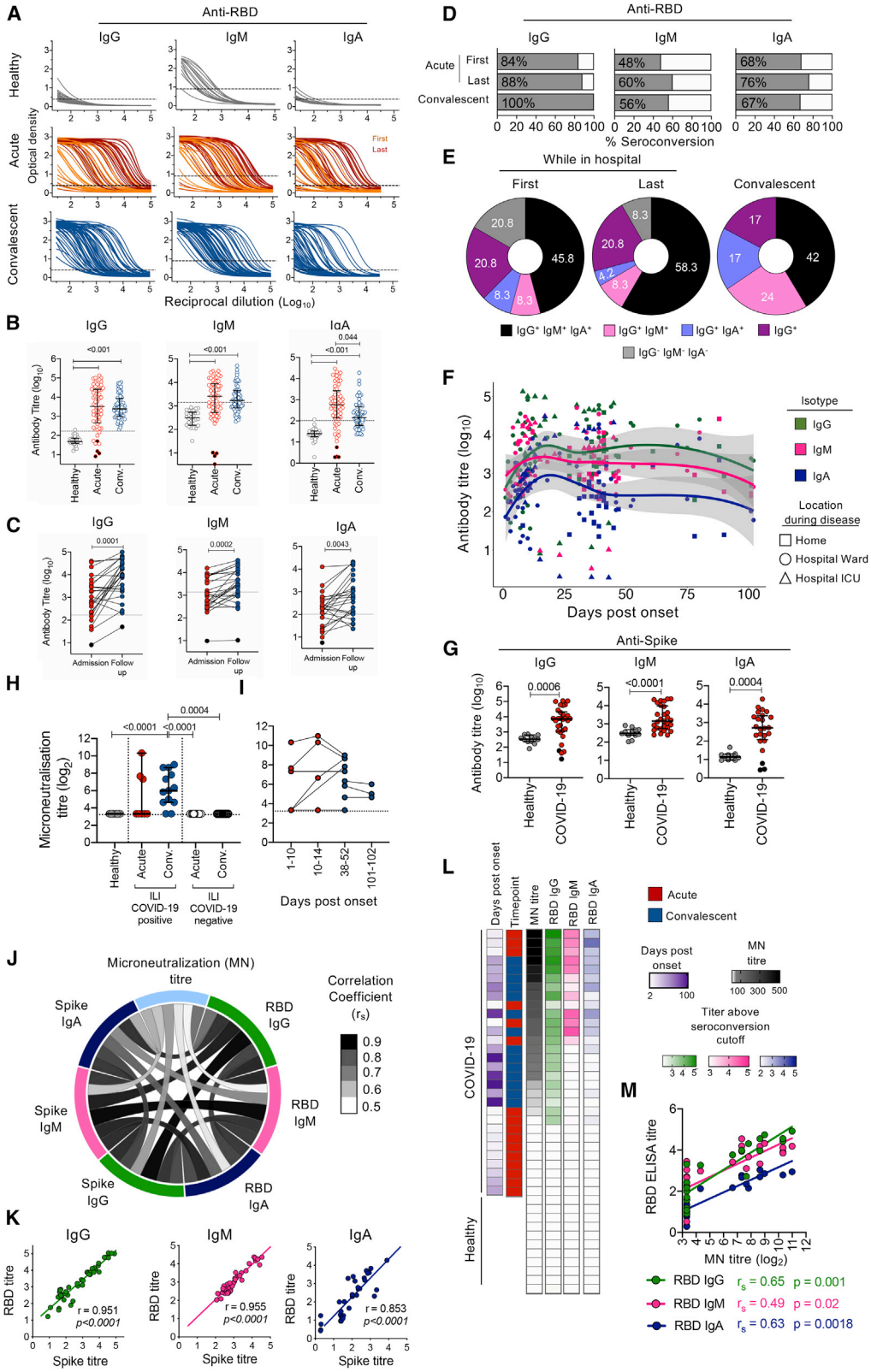

(legend on next page)

significantly higher in acute (log_{10} median titer 3.52 IgG, 3.41 IgM, 2.77 IgA) and convalescent COVID-19 samples (log_{10} median titer 3.38 IgG, 3.24 IgM, 2.15 IgA) compared to those in healthy, non-exposed individuals (log_{10} median titer 1.68 IgG, 2.49 IgM, 2.15 IgA) (Figure 3B). While IgG and IgM titers were maintained at similar levels between acute and convalescent samples, IgA titers had significantly decreased by convalescence. Paired analysis confirmed a significant increase in antibody titers from the first sampling following admission to just before discharge or at convalescence for all 3 isotypes (Figure 3C). At the first acute blood collection, 84%, 48%, and 68% of individuals seroconverted (log_{10} antibody titer > mean + 2× SD of healthy individuals) for RBD-specific IgG, IgM, and IgA antibodies, respectively (Figure 3D). IgG seroconversion rates increased to 88% and 100% at the last acute blood collection and at convalescence, respectively, although IgM and IgA were maintained at similar frequencies (Figure 3D). In addition, the proportion of individuals with undetectable RBD-specific IgG, IgM, or IgA antibodies decreased from 20.8% during the acute phase to 0% at convalescence, with 100% of convalescent donors having at least an IgG response to RBD (Figure 3E). Consistently, the levels of RBD-specific IgG, IgM, and IgA antibodies rapidly increased in the first 3 weeks, with IgG and IgM levels being maintained between days 25 and 102 (Figure 3F). We observed a trend toward decreased IgA levels from day 25 onward (Figure 3F), but only in 3/25 patients. In addition, we measured Spike-specific antibodies by ELISA and detected higher IgG, IgM, and IgA antibodies against Spike in pooled acute and convalescent COVID-19 samples compared to healthy donors (Figure 3G).

To determine the neutralizing activity of SARS-CoV-2-specific antibodies, a microneutralization (MN) assay was performed using live SARS-CoV-2 virus infection of Vero cells.[11] Neutralizing antibodies were detected at a low frequency in 3/8 acute patients, but were more prevalent in 11/13 convalescent samples, the latter being significantly higher than healthy non-exposed and hospitalized non-COVID patient control groups (Figure 3H). Neutralizing activity increased from the acute to the convalescent phase and was still detectable in 3/3 convalescent donors sampled at ~100 days post-symptom onset (Figure 3I). Several antibody measurements correlated significantly with each other (Figures 3J–3M). When we ranked COVID-19 patients according to the neutralizing activity of SARS-CoV-2-specific antibodies, COVID-19 patients with the highest MN activity had high levels of RBD-specific IgM, IgG, and IgA, suggesting that engagement of a broad range of antibody isotypes may lead to improved neutralizing activity (Figure 3L). Importantly, antibodies against Spike and neutralizing antibody titers correlated with RBD-specific IgG, IgM, and IgA antibodies (Figures 3J, 3K, and 3M).

Activated PD-1$^+$ICOS$^+$ cT$_{FH}$1 cells correlate with robust humoral immunity

Consistent with previous observations, our analyses of SARS-CoV-2-specific antibodies demonstrated considerable variability among acute COVID-19 patients (Figure 3B). To understand the basis of such variability and identify potential predictors of antibody signatures, we dissected correlations between antibody responses (RBD or Spike, IgG, IgM, or IgA, MN) and immune populations involved in humoral immunity, ASCs, and activated cT$_{FH}$1, cT$_{FH}$2/cT$_{FH}$17, T$_H$1, and T$_H$2/T$_H$17 subsets (Figure 4A). We found significant positive correlations between the number of ASCs and MN titers (r_s = 0.543) and Spike-specific IgA antibodies (r_s = 0.597). The number of activated cT$_{FH}$1 cells positively correlated with the levels of RBD- and Spike-specific antibodies of all 3 isotypes (r_s > 0.288 for RBD, r_s > 0.549 for Spike) and MN titers (r_s = 0.659). We observed no significant correlations between CXCR3$^-$ cT$_{FH}$2/cT$_{FH}$17 cells or activated CD4$^+$ T cells not belonging to the CXCR5$^+$ T$_{FH}$ lineage and antibody responses.

To evaluate the potential of immune populations as predictors of the acute antibody response, we performed linear regression of each immune cell population against each antibody measurement and consistently found ASCs and activated cT$_{FH}$1 cells, but not other CD4$^+$ T cell subsets, as significant positive predictors of matched RBD-specific, Spike-specific, and MN titers (Figure 4B). While in some instances, the correlations with immune

Figure 3. Antibody signatures against RBD and Spike protein in acute and convalescent COVID-19

(A) ELISA titration curves against the SARS-CoV-2 RBD for IgG, IgM, and IgA in healthy donors (n = 25–26), acute (n = 61), and convalescent (n = 63) COVID-19 patients. Dotted line indicates the cutoff for endpoint titer determination.

(B) Endpoint titers of SARS-CoV-2 RBD antibodies, in which the dotted line indicates the seroconversion titer.

(C) Paired endpoint titers of SARS-CoV-2 RBD antibodies from COVID-19 patients (n = 25) at admission and follow-up.

(D and E) Seroconversion rates (D) and (E) isotype profiles for RBD-specific IgG, IgM, and IgA at acute and convalescent time points.

(F) Kinetics of RBD-specific antibodies for IgG, IgM, and IgA. LOESS regression lines with 95% confidence intervals shaded in gray are shown.

(G) Endpoint titers of SARS-CoV-2 Spike antibodies for IgG, IgM, and IgA in healthy donors (n = 10–12) and COVID-19 (n = 24–30) plasma.

(H) Microneutralization titers against SARS-CoV-2 in healthy (n = 21), COVID-19$^+$ (acute n = 8, convalescent n = 13) and COVID-19$^-$ (acute n = 13, convalescent n = 7) sera.

(I) Longitudinal analysis of microneutralization titers from days postsymptom onset.

(J) Circos plot depicting correlations (links) between different antibody measurements (edges). Only significant ($p < 0.05$) correlations are shown. The color of the links represents the strength of the correlation based on the Spearman correlation coefficient, n = 24 samples for which all antibody measurements were available.

(K) Correlation between RBD-specific and Spike-specific titers for IgG (n = 44), IgM (n = 41), and IgA (n = 34) samples.

(L) Heatmap of microneutralization and ELISA titers. Each row represents a different sample with their matched measurements.

(M) Correlation between microneutralization titers and RDB-specific titers for each isotype (n = 22 samples per isotype). Median and interquartile range (IQR) are shown throughout.

(B and G) Black-filled symbols indicate patient no. 1-088 with rituximab treatment who was not included for statistical analysis. Statistical significance was assessed with a Kruskal-Wallis test with Dunn's correction for multiple comparisons (B and H). (C) Wilcoxon matched-pairs signed rank test or a Mann-Whitney test (G). (K and M) Spearman correlation coefficients and p values shown.

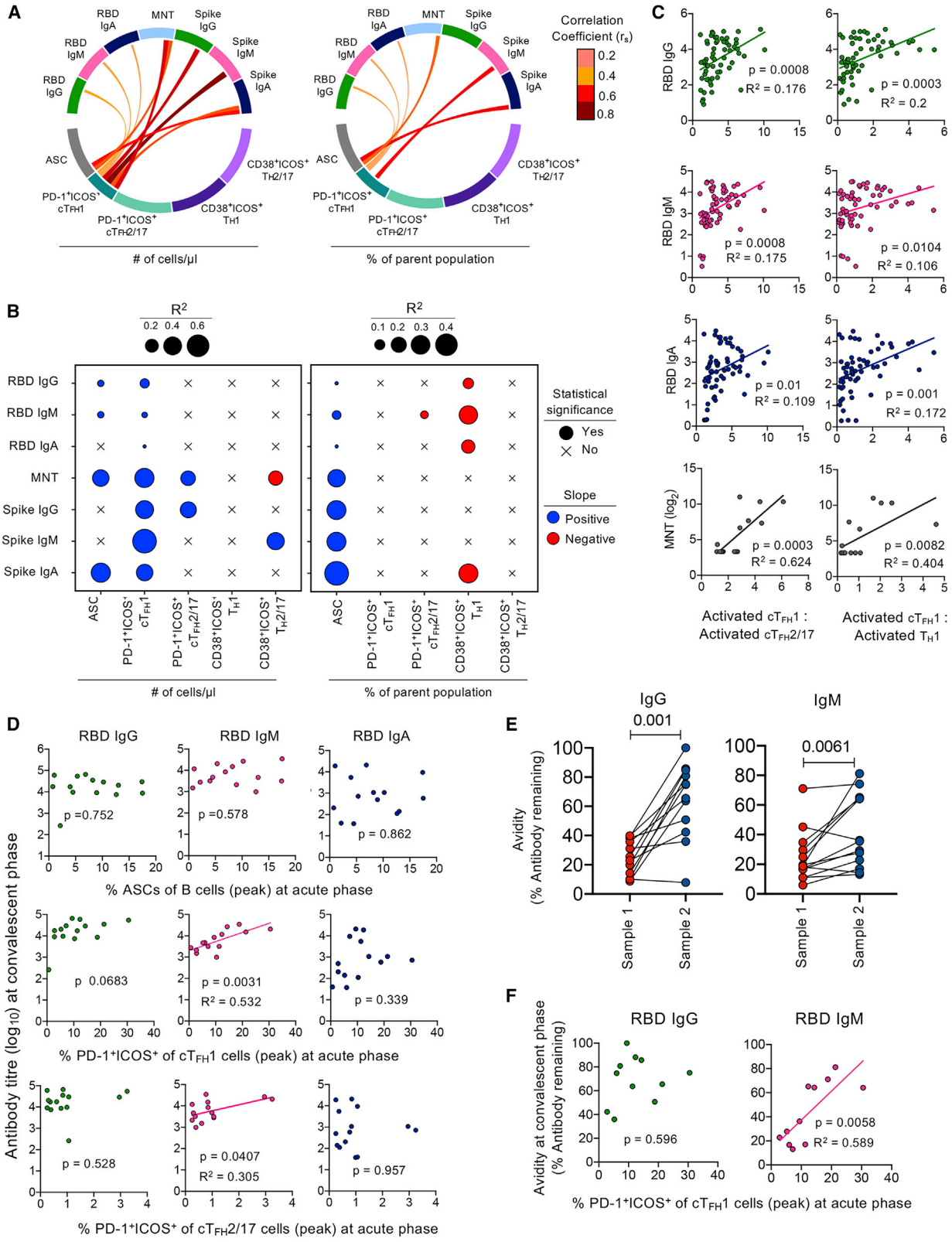

(legend on next page)

populations were strong (e.g., activated $cT_{FH}1$ cells and Spike-specific IgM, R^2 = 0.73) or modest (e.g., ASC and MN titers [MNTs], R^2 = 0.36), they were weak for RBD-specific antibodies (R^2 < 0.2). Activation of non-T_{FH} cells was also a negative predictor of RBD-specific antibodies (Figure 4B). We observed that higher ratios of activated $cT_{FH}1$ cells to activated $cT_{FH}2$/$cT_{FH}17$ cells or activated $cT_{FH}1$ cells to activated T_H1 cells were significant positive predictors of matched MNTs (R^2 = 0.624 and R^2 = 0.404, respectively) and RBD-specific antibodies for all isotypes, albeit to a lesser extent (R^2 < 0.2) (Figure 4C).

As our results are based on immune and antibody analyses from longitudinal samples during acute COVID-19, and are consistent with data in convalescent individuals,[11] we determined whether immune populations measured at the acute phase could act as biomarkers for convalescent antibody responses. We analyzed paired longitudinal data from individuals with acute immune and convalescent RBD antibody data (n = 14 patients) using the peak value of the immune cell population when >1 acute measurement was available. The levels of activated $cT_{FH}1$ cells were significant positive predictors of convalescent RBD-specific IgM antibodies, by both proportion and number of cells (R^2 = 0.531 and R^2 = 0.37, respectively) (Figures 4D and S10A). Interestingly, while a similar result was also observed for the proportion of activated $cT_{FH}2$/$cT_{FH}17$ cells (p = 0.0407, R^2 = 0.305), this was not observed for cell numbers. Neither the proportion nor the numbers of acute ASCs were significant predictors of convalescent RBD-specific antibodies. Overall, activated $cT_{FH}1$ cells in the acute phase were associated with greater levels of RBD-specific IgM antibodies at convalescence.

Having shown that activated PD-$1^+$$ICOS^+$ $cT_{FH}1$ cells correlate with RBD-, Spike-, and MN antibody titers (thus magnitude), we asked whether these $cT_{FH}1$ cells could also be associated with qualitative features of antibodies. We measured the avidity of RBD-specific IgG and IgM antibodies using a urea dissociation assay. In paired COVID-19 plasma samples (n = 13) obtained >7 days apart, we found a significant increase in IgG and IgM avidity (percentage of antibody remaining after 6 M urea treatment) in the second plasma sample (Figures 4E and S10B). Avidity also increased with time, where RBD-specific IgG antibodies detected within the first week had significantly lower avidity than samples obtained ≥3 weeks later (Figure S10C). The proportion of PD-$1^+$$ICOS^+$ $cT_{FH}1$ cells at the acute time points positively correlated with antibody avidity for RBD IgM (p = 0.0058, R^2 = 0.589), but not RBD IgG, at convalescence (Figure 4F). Thus, activated PD-$1^+$$ICOS^+$ $cT_{FH}1$ cells in acute COVID-19 correlate with robust humoral immunity, in both a quantitative (RBD-specific, S-specific, and MN titers) and qualitative (IgM avidity) sense. Overall, robust antibody responses elicited during SARS-CoV-2 infection were associated with T_{FH} activation; thus, cT_{FH} responses may be valuable as potential biomarkers in vaccine clinical trials.

Hyperactivated $CD38^+$$HLA\text{-}DR^+$ innate and adaptive immune cells, sIL-6R, and IL-18 during severe COVID-19

We selected 19 key innate and adaptive immune subsets identified to be prominent in acute versus convalescent COVID-19 samples (Figure 2) for broader analyses, including acute datasets for the 14 cytokines/chemokines and RBD-specific IgG/IgM/IgA antibodies (total 36 features), while correcting for multiple comparisons (Figure 5A), to elucidate immune mechanisms driving disease severity. In fact, 9/36 (25%) immune features were significantly enhanced in severely ill patients (ICU versus ward), including activated $CD38^+$$HLA\text{-}DR^+$$CD8^+$, $CD38^+$$HLA\text{-}DR^+$$CD4^+$, $CD38^+$$HLA\text{-}DR^+$ γδ T cells, PD-$1^+$$ICOS^+$ $cT_{FH}1$ and $cT_{FH}2$/$cT_{FH}17$ cells, $HLA\text{-}DR^+$ NK cells, patrolling $CD16^+$ monocytes, and higher levels of IL-18 and sIL-6R, reminiscent of prolonged and high expression of $CD38^+$$HLA\text{-}DR^+$ on $CD8^+$ T cells associated with mortality in H7N9-infected patients.[26] In the hospitalized moderate patients who did not require ICU care, classical $CD14^+$ monocytes were higher and RBD-specific antibodies were not significantly different (Figure 5A). Nevertheless, the 10 features were sufficient to clearly separate samples from moderate (ward) and severe (ICU) patients by principal-component analysis (PCA), whereby the ward and ICU groups were separated along PC1 (explaining 41.4% of variance) and ICU samples further separated along PC2 (accounting for 18.1% of variance) (Figure 5B).

Hyperactivation of immune cell subsets in ICU patients was further demonstrated by dissecting immune subsets individually. This was evident when analyzing the proportion of activated $CD38^+$$HLA\text{-}DR^+$ immune sets (Figure 5C). Markedly higher proportions of $CD38^+$$HLA\text{-}DR^+$$CD4^+$ (18.25% versus 2.84%), $CD38^+$$HLA\text{-}DR^+$$CD8^+$ (28.9% versus 5.55%), $CD38^+$$HLA\text{-}DR^+$

Figure 4. cTfh1 cells are associated with acute and convalescent antibody levels

(A) Circos plot depicting correlations (links) between different antibody measurements and various immune cells from acute COVID-19 samples (n = 61). Correlations for absolute numbers (left) and proportions of cells (right). Only significant (p < 0.05) correlations are shown. The color of the links represents the strength of the correlation based on the Spearman correlation coefficient.

(B) Summary of linear regression analysis between different antibody measurements against various immune cells from acute COVID-19 samples.

(C) Linear regression analysis of acute RBD-specific titers (n = 60–61) for each isotype or microneutralization titers (MNTs, n = 16) and the ratio of acute activated $cT_{FH}1$ cells (PD-$1^+$$ICOS^+$$CXCR3^+$$CXR5^+$$CD4^+$ T cells) and activated $cT_{FH}2$/$cT_{FH}17$ cells (PD-$1^+$$ICOS^+$$CXCR3^-$$CXR5^+$$CD4^+$ T cells, left) or activated T_H1 cells ($CD38^+$$ICOS^+$$CXCR3^+$$CXR5^-$$CD4^+$ T cells, right).

(D) Linear regression analysis of the proportion of acute ASCs, PD-$1^+$$ICOS^+$ $cT_{FH}1$ or PD-$1^+$$ICOS^+$ $cT_{FH}2$/$cT_{FH}17$ cells and paired convalescent RBD-specific titers for each isotype, n = 14.

(E) Avidity analysis for IgG and IgM RBD-specific antibodies in paired samples. Frequency of antibody binding after treatment with 6 M urea compared to without treatment is shown. Presented are results from a 1:100 plasma dilution for IgG and a 1:316 dilution for IgM. Samples 1 and 2 were collected 7–70 days apart. Statistical significance was assessed with a Wilcoxon matched-pairs signed rank test, n = 13.

(F) Linear regression analysis of the proportion of acute PD-$1^+$$ICOS^+$ $cT_{FH}1$cells and paired convalescent avidity measurements for IgG and IgM RBD-specific antibodies, n = 11.

(A and B) RBD IgG/M/A n = 60–61, MNTs n = 16, Spike IgG/IgM/IgA n = 12–15.

CellPress
OPEN ACCESS

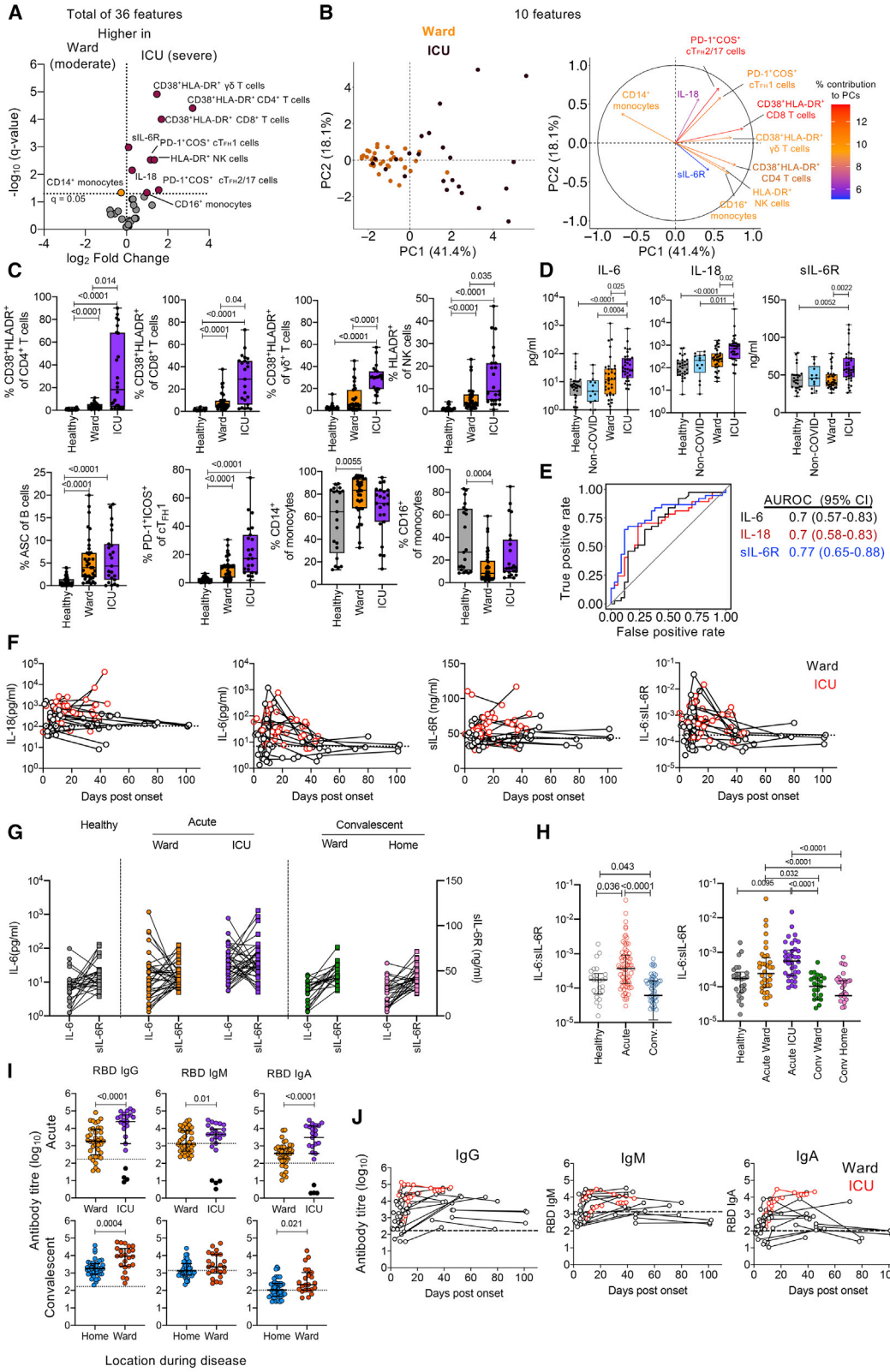

(legend on next page)

γδ T cells (30.3% versus 5.48%), HLA-DR$^+$ NK cells (8.87% versus 3.63%), and patrolling CD16$^+$ monocytes (12.8% versus 8.26%) were found in the ICU compared to the ward group. Strikingly, in some ICU patients, levels of hyperactivated CD38$^+$HLA-DR$^+$ CD4$^+$ T cells constituted ~80% of all blood CD4$^+$ T cells, while up to 50% of all blood CD8$^+$ T cells, NK cells, and γδ T cells were found in some ICU patients (Figure 5C) , indicating a non-specific bystander mode of activation. Moreover, immune cell activation was clearly higher in ICU patients as the total numbers for each parent population were comparable between severity groups (Figure S11). Immune clustering further identified significant differences between ICU and ward, including higher levels of CD38$^+$HLA-DR$^+$ neutrophils, eosinophils, NK cells, γδ, CD4$^+$, and CD8$^+$ T cells in ICU samples (Figure S12). We also found significantly higher neutrophil:lymphocyte and neutrophil:T cell ratios in ICU patients (Figure S12).

Concomitantly, we also observed significantly different levels of IL-6, IL-18, and sIL-6R (Figure 5D). ICU patients had significantly higher levels of IL-18 (ward 238.8 pg/mL, ICU 700.9 pg/mL) and sIL-6R (ward 40.37 ng/mL, ICU 57.9 ng/mL) (Figures 5D and S11C). Importantly, we observed higher IL-6 levels in ICU compared to ward patients (ward 11.95 pg/mL, ICU 28.8 pg/mL, $p = 0.025$). Analysis of the area under the receiver operating characteristic (AUROC) curve indicated that sIL-6R (AUROC = 0.77), IL-18 (AUROC = 0.7), and IL-6 (AUROC = 0.7) are potentially predictive of ward versus ICU cases (Figure 5E).

Longitudinal analyses verified high levels of IL-18, IL-6, and sIL-6R in ICU patients when compared to the ward patients over time, while the ratio of IL-6:sIL-6R was variable among ICU and ward patients (Figures 5F and 5H). When paired IL-6 and sIL-6R data were analyzed, high IL-6 levels in acute COVID-19 did not imply high sIL-6R levels (Figures 5G and 5H). Conversely, it appeared that acute (both ward and ICU) COVID-19 samples with the highest IL-6 plasma concentration had modest levels of sIL-6R. These results have important implications for IL-6/IL-6R immunotherapies and need to be further investigated in larger COVID-19 cohorts.

Further focus on the association of disease severity with SARS-CoV-2 antibody responses revealed significantly higher levels of RBD-specific IgG, IgM, and IgA antibodies in ICU than in ward patients (Figures 5I and 5J), in agreement with previous reports.[8] Interestingly, convalescent patients who were originally hospitalized with COVID-19 had significantly higher RBD-specific IgG and IgA antibodies than those who were cared for at home (Figure 5I). ICU patients had higher cT$_{FH}$1 responses, albeit insignificant in the proportions and numbers, but comparable ASC responses to those of the ward patients (Figure 5C).

Thus, severe COVID-19 was associated with overwhelming immune activation of innate, adaptive lymphoid and myeloid compartments, higher antibody responses supported by greater cT$_{FH}$1 activation, and enhanced levels of IL-6, IL-18, and sIL-6R. Thus, IL-18 and CD38$^+$HLA-DR$^+$ expression may be useful biomarkers of COVID-19 severity, while sIL-6R levels are relatively low in COVID-19 patients (with the exception of ICU patients), in comparison to the levels detected in cancer patients (up to 195 ng/mL).[29]

IL-6/sIL-6R and IL-18 hypercytokinemia associated with dysregulation of innate and adaptive immunity

To gain insights into the basis of the immune hyperactivation profiles, we performed correlation analysis of 14 cytokines and 22 immune cell populations (Figures 6A–6C). IL-6 positively correlated with IL-8, IL-18, and IFN-γ (Figure 6A), where elevated levels of IL-6 were reported for severe influenza disease and mortality.[30,31] Consistent with other studies,[2] we found that IL-6 negatively correlated with lymphocyte numbers in blood (Figure 6B), possibly reflecting the efflux of immune cells from blood to the site of infection. Importantly, we also found positive correlations between levels of IL-6 or IL-18 with T cells and NK cell hyperactivation (Figures 6B and 6C). IL-6 and IL-18 significantly correlated with the proportion of CD38$^+$HLA-DR$^+$ γδ T cells ($r_s = 0.37$, $p = 0.004$ and $r_s = 0.53$, $p < 0.0001$, respectively) and IL-18 significantly correlated with the proportion of CD38$^+$ICOS$^+$ CD4$^+$ T cells ($r_s = 0.29$, $p = 0.028$) (Figure 6C). We also found that the proportions of CD14$^+$ and CD16$^+$ monocytes were positively and negatively associated with the levels of MCP-1, respectively. Significant correlations were detected between the levels of sIL-6R and CD38$^+$HLA-DR$^+$γδ T cells ($r_s = 0.35$, $p = 0.008$), CD38$^+$HLA-DR$^+$CD8$^+$ T cells ($r_s = 0.32$, $p = 0.012$), CD38$^+$HLA-DR$^+$CD4$^+$ T cells ($r_s = 0.42$, $p = 0.0013$), and HLA-DR$^+$ NK cells ($r_s = 0.36$, $p = 0.006$). Interestingly, significant correlations were found between sIL-6R with RBD IgG,

Figure 5. sIL-6R and IL-18 are predictors of severe COVID-19

(A) Volcano plot of differential immune profiles between acute ward and ICU samples based on 19 manually gated immune cell populations, 14 cytokines/chemokine, and 3 RBD-antibody titers.

(B) PCA analysis of ward and ICU samples using the 10 significant features. Individual samples color-coded based on severity group (left) and the contribution of each feature to the principal components (right) are shown.

(C) Proportion of acutely activated lymphocytes and monocytes in ward (n = 36–37) and ICU samples (n = 23) based on manual gating strategy.

(D) Acute cytokine levels in healthy controls (n = 32), non-COVID-19 influenza-like illness (ILI) (n = 13), ward (n = 36), and ICU samples (n = 36).

(E) AUROC analysis of IL-6, IL-18, and sIL-6R for discriminating ward versus ICU samples.

(F) Longitudinal tracking of cytokine levels in ward and ICU patients.

(G) Matched IL-6 and IL-6R levels in acute ward and ICU patients.

(H) IL-6:IL-6R ratios in healthy, acute (ward or ICU), and convalescent individuals.

(I) Endpoint titers of SARS-CoV-2 RBD antibodies for IgG, IgM, and IgA in acute COVID-19 plasma samples from individuals in hospital ward or ICU during the acute phase (top) or in convalescent plasma samples from individuals who were at home (n = 40) or in the hospital ward (n = 24) during acute COVID-19.

(J) Longitudinal antibody levels of ward and ICU matched patient samples for RBD-specific IgG, IgM, and IgA. The dotted line represents the seropositivity cutoff value for each isotype (antibody titer > mean + 2× SD of healthy individuals).

(C, D, H, and I) Statistical significance was assessed with a Kruskal-Wallis test with Dunn's correction for multiple comparisons; median and IQR are shown throughout.

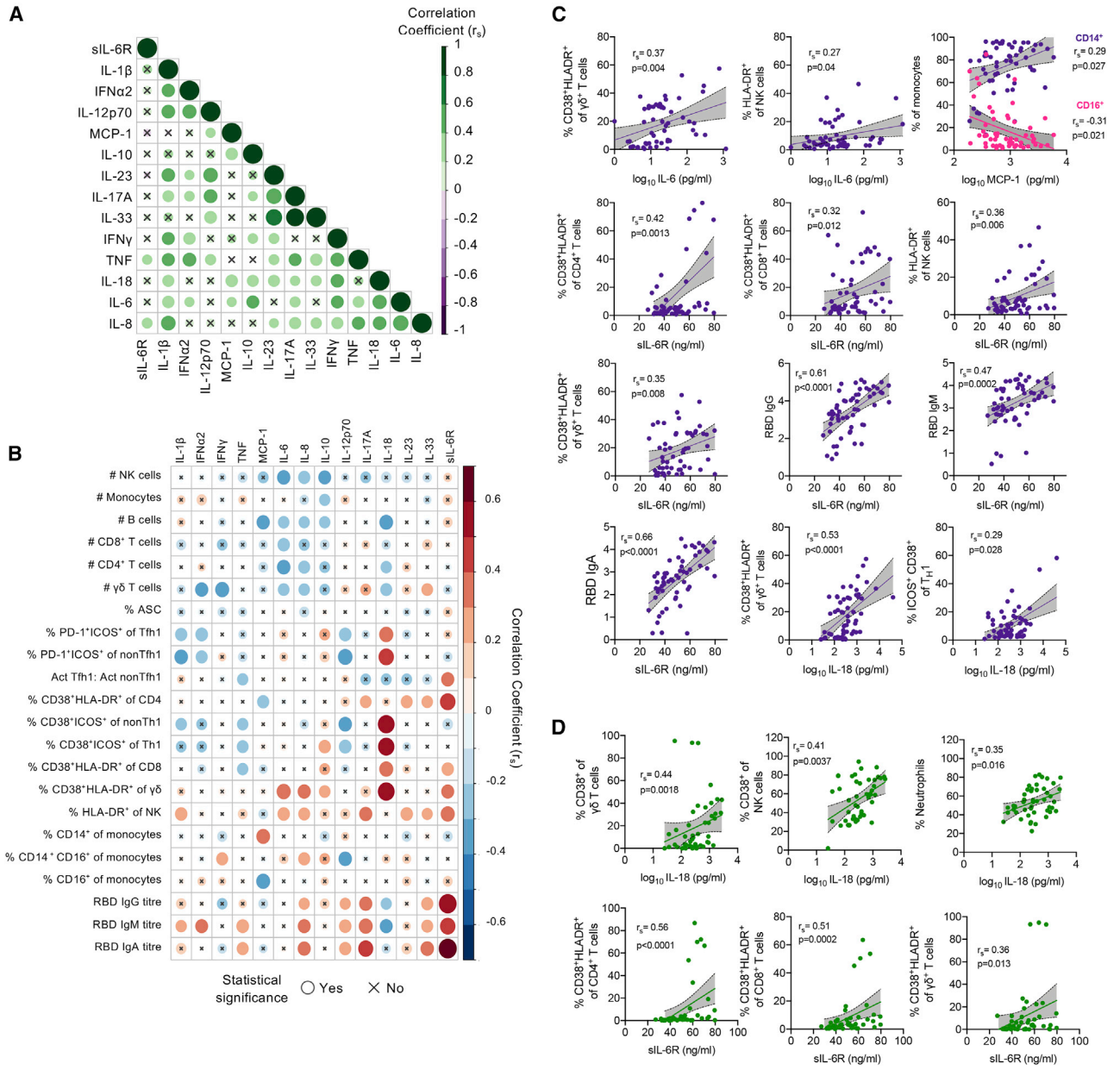

Figure 6. IL-6, sIL-6R, and IL-18 hypercytokinemia are associated with dysregulation of innate and adaptive immunity

(A) Correlation matrix of cytokines in all acute samples. Statistical significance was defined as false discovery rate (FDR)-corrected p value q < 0.1.

(B) Heatmap summarizing the correlations between cytokine levels and immune populations in acute COVID-19 based on manual gating strategy. Statistical significance was defined as FDR-corrected p value q < 0.1.

(C and D) Representative plots of significant correlations between cytokine levels and immune cell populations from acute samples (n = 57) based on manual gating strategy and RBD-antibody titers (C) and FlowSOM analysis (D).

IgM, and IgA titers, with those being higher in ICU samples. We found consistent results when analyzing the proportions of immune cell clusters determined by FlowSOM, with IL-6 and IL-18 positively correlating with activation of myeloid cells, T cells, and NK cells (Figures 6D and S13).

Overall, our study provides a comprehensive map of longitudinal immunological responses in COVID-19 patients at acute and convalescent phases of SARS-CoV-2 infection (Figure S14) and demonstrates prototypical antiviral immunity in mild/moderate cases, but dysregulated immune hyperactivation in severe COVID-19. Our analyses unify the levels of IL-6, sIL-6R, and IL-18 and their association with severe COVID-19 with the immune hyperactivation profiles at the cellular level characterized by high CD38 expression (Figure 6D).

DISCUSSION

Immune responses toward non-severe SARS-CoV-2 infection resemble a prototypical antiviral immune response, with transient activation of innate myeloid and lymphoid populations at the acute phase. These include $cT_{FH}1$ cells, T_H1 $CD4^+$ T cells, highly cytotoxic $CD38^+HLA\text{-}DR^+CD8^+$ T cells, SARS-CoV-2-specific B cells, and antibodies. This is followed by the subsequent contraction of immune responses after disease resolution, as shown by us and others,[3,6,11] similar to other acute respiratory infections.[27,32] Despite prototypical immune responses found in mild/moderate COVID-19 cases, profoundly dysregulated innate and adaptive immunity underlie severe COVID-19, including elevated plasma IL-18 and sIL-6R levels, and hyperactivation of innate, adaptive, and myeloid compartments in ICU COVID-19 patients. Our study provides a comprehensive map of longitudinal immunological responses in COVID-19 patients at acute and convalescent phases and integrates key cellular pathways of complex perturbed immune networks underpinning critical COVID-19, providing important insights into biomarkers and immunotherapies.

Our analysis of humoral immune responses to SARS-CoV-2 demonstrated generation of RBD- and Spike-specific IgG, IgM, and IgA antibodies and their correlation with SARS-CoV-2 neutralization activity. Early activation of ASCs, likely of extrafollicular origin, was associated with Spike-specific IgG, IgM, and IgA antibodies, antibody neutralization activity, and, to a lesser extent, RBD-specific titers. Our data are in agreement with the emergence of IgG, IgM, and IgA ASC in COVID-19 patients, some specific for non-Spike antigens (e.g., nucleocapsid protein), which may explain the lack of a strong correlation between ASCs and RBD-specific antibodies in our cohort and other studies.[4,6]

Activation of $cT_{FH}1$ cells is an important correlate of antibody responses following influenza vaccination,[25] yellow fever,[33] and hepatitis C virus (HCV).[34] Although the lack of $Bcl6^+$ T_{FH} cells in lymphoid organs of severely ill COVID-19 patients was shown,[35] cT_{FH} response at the convalescent phase was associated with antibody responses to SARS-CoV-2.[11] Our analysis extends this observation to the acute phase and importantly associates acute $cT_{FH}1$ responses with convalescent IgM antibody titers. It also demonstrates an association between $cT_{FH}1$ responses and an increase in antibody avidity, potentially reflecting affinity maturation in germinal centers. We found that greater activation of $cT_{FH}1$ cells relative to other $CD4^+$ T cell subsets was associated with greater RBD-specific responses and better neutralization activity. Our findings thus support the use of adjuvants that can induce strong T_{FH} responses to improve vaccine efficacies. In humans, GLA-SE in the malaria vaccine induced greater cT_{FH} responses than alum,[36] while in non-human primates and mice, MF59 enhanced cT_{FH} activation and antibody responses to HIV-1 and influenza, respectively.[37,38] Since some of the SARS-CoV-2 vaccines in clinical trials are formulated with alum or MF59,[39] it may be important to compare immunogenicity across vaccine formulations.

IL-6 is the key driver of an inflammatory cascade in severe COVID-19;[1,2,20] thus, therapies targeting sIL-6R are in clinical trials for SARS-CoV-2 infection. Two humanized monoclonal antibodies against IL-6R, tocilizumab (Roche) and sarilumab (Sanofi), safely used for autoimmune diseases, are being evaluated in COVID-19, but neither has met the primary endpoints.[40,41] There have been limited analyses of sIL-6R in acute and convalescent COVID-19 patients. Surprisingly, although the plasma sIL-6R levels were significantly elevated in severe COVID-19 compared to moderate disease, they remained within the healthy range (up to 80 ng/mL).[42] Interestingly, while IL-6 was considerably elevated in acute COVID-19 samples, patients with the highest IL-6 concentrations had only modest sIL-6R levels, and levels of sIL-6R did not correlate with IL-6 or any other cytokines. In addition, the elevated levels of IL-6 and IL-18 found in critically ill COVID-19 patients are in the same range as those of patients with non-COVID-19 acute respiratory distress syndrome (ARDS) or sepsis.[43] Our results suggest that patients should be screened for both IL-6 and sIL-6R before the initiation of anti-IL-6R therapy, especially since critically ill COVID-19 patients receiving anti-IL-6R therapies may be at higher risk of nosocomial infections.[44] Interestingly, the levels of IL-6 correlate with lymphocytopenia in our cohort and others,[2] and treatment with anti-sIL-6R therapies can restore lymphocyte numbers. We also found a correlation between sIL-6R and the activation of $CD8^+$, $CD4^+$, and $\gamma\delta$ T cells. Since activated T cells are considered a major source of sIL-6R[45] and severe COVID-19 presents with T cell hyperactivation, this may explain the elevated levels of sIL-6R and support the idea that sIL-6R may be an informative biomarker.

IL-18 was also associated with COVID-19 severity in our analysis and another report.[7] We found a correlation between IL-18 levels and the activation of innate NK cells and $\gamma\delta$ T cells, as well as $CD4^+$ and $CD8^+$ T cells, which is consistent with the potential of IL-18/IL-18R signaling to induce bystander activation of innate and adaptive T cells.[46–48] These observations unify the elevated levels of cytokines, such as IL-6 and IL-18, and their signaling pathways with hallmark observations of severe COVID-19 disease, like hyperactivation of T cells and elevated antibody levels, and thus provide insights into underlying mechanisms and a potential therapeutic role for anti-IL-18 therapies.[49,50] The use of dexamethasone showed benefits in severely ill COVID-19 patients,[15] consistent with immune hyperactivation observed in those patients. However, neither sIL-6R nor IL-18 were universally higher in ICU patients, nor do they fully explain the immunological differences between ward and ICU samples. Our data further highlight the need for multiparameter immune profiling of severe COVID-19 patients to identify and appropriately select personalized immune-modulatory treatments.

The hyperactivation of immune cells in severe ICU cases, suggestive of substantial immune dysregulation, was clearly evident from elevated CD38 expression on a broad range of immune cells. The upregulation of CD38 and HLA-DR on T cells in COVID-19 in our study and by others[4,6,8] is consistent with the high levels of $CD38^+HLA\text{-}DR^+$ $CD8^+$ T cells observed in HIV,[51] Ebola,[52] HCV,[53] and dengue.[54] Our data from severe COVID-19 cases support our previous study showing high and prolonged proportion of $CD38^+HLA\text{-}DR^+$ $CD8^+$ T cells (up to 50% for $\sim$30 days) in patients who died from avian A/H7N9 influenza.[26] Numerically, 50%–80% of $CD38^+HLA\text{-}DR^+$ T cells found

in the peripheral blood of severe H7N9 or COVID-19 cases unlikely reflect epitope-specific T cell activation. In fatal H7N9 cases, delayed clonal expansion of H7N9-specific $CD8^+$ T cells and distinct transcriptome signatures of $CD38^+HLA\text{-}DR^+$ $CD8^+$ T cells were indicative of bystander activation. In COVID-19 patients, such T cell hyperactivation was associated with elevated cytokine levels that may drive bystander activation, similar to H7N9 hypercytokinemia.[31] Thus, while rapid and transient $CD38^+HLA\text{-}DR^+$ expression can be detected in patients with relatively rapid recovery,[26] prolonged and high expression levels are associated with severe and/or fatal outcomes in COVID-19 and avian H7N9.[3,26] Given that high CD38 expression is a poor prognostic factor in cancers and HIV,[55] monitoring CD38 expression on a wide range of immune cells may be a useful marker of immune hyperactivation and disease progression in COVID-19.

Limitations of study

We recognize that some of the analyses performed are limited to a relatively small number of patients available. This is particularly relevant to the analysis of ICU samples, the longevity analysis of antibodies, and the analysis of neutralizing titers. In addition, we could not stratify our cohort based on age groups or the use of immunomodulatory treatments, which should be the focus of future studies.

STAR★METHODS

Detailed methods are provided in the online version of this paper and include the following:

- KEY RESOURCES TABLE
- RESOURCE AVAILABILITY
  - Lead contact
  - Materials availability
  - Data and code availability
- EXPERIMENTAL MODEL AND SUBJECT DETAILS
- METHOD DETAILS
  - Whole blood flow cytometry
  - RBD and Spike protein ELISAs
  - Antibody avidity assay
  - Microneutralisation assay
  - Cytokine analysis
- QUANTIFICATION AND STATISTICAL ANALYSIS
  - Computational flow cytometry analysis
  - Statistical analyses

SUPPLEMENTAL INFORMATION

Supplemental Information can be found online at https://doi.org/10.1016/j.xcrm.2021.100208.

ACKNOWLEDGMENTS

We thank all of the participants in the study and Jeni Mitchell, Robyn Esterbauer, Hannah Kelly, Jane Batten, Helen Kent, Jill Garlick, Janine Roney, and Anne Paterson for support with the cohorts. This research included samples from the Sentinel Travelers Research Preparedness Platform for Emerging Infectious Diseases (SETREP-ID). We acknowledge the SETREP-ID investigators and sites, Barbara Scher for setting up the ethics and governance for SETREP-ID, the Australian Partnership for Preparedness Research for Infectious Disease Emergencies (APPRISE) for funding of SETREP-ID, and Ajantha Solomon, Judy Chang, and Ashanti Dantanaranaya for SETREP-ID biobanking. This work was supported by the NHMRC Leadership Investigator Grant to K.K. (no. 1173871); the NHMRC Program Grant to D.L.D. (no. 1132975); the Research Grants Council of the Hong Kong Special Administrative Region, China (no. T11-712/19-N) to K.K.; the Jack Ma Foundation to K.K., K.S., D.I.G., and A.W.C.; the a2 Milk Foundation to K.S.; the Victorian Government MRFF award (no. 2002073) to S.J.K., D.I.G., and A.K.W.; MRFF Award (no. 1202445) to K.K.; MRFF Award (no. 2005544) to K.K., S.J.K., J.J., A.W.C., and A.K.W.; NHMRC program grant no. 1149990 to S.J.K.; NHMRC project grant no. 1162760 to A.K.W.; NHMRC program grant (no. 1071916) to K.K. and D.C.J.; NHMRC program grant (no. 1113293) to D.I.G.; the Merridew Foundation to N.J.C.K. and D.L.D.; NHMRC Principal Research Fellowship (no. 1137285); NHMRC Investigator grant (no. 1177174) to K.S.; NHMRC Career Development Fellowship (no. 1145033) to S.Y.C.T.; and NHMRC Senior Principal Research Fellowships (nos. 1117766 and 1136322) to D.I.G. and S.J.K. S.R.L. is supported by an NHMRC Program Grant (no. 1149990) and a Practitioner Fellowship (no. 1135851). L.H., J.R.H., and W.Z. are supported by the University of Melbourne International Research Scholarship and the Melbourne International Fee Remission Scholarship. X.J. is supported by the China Scholarship Council-University of Melbourne Joint Scholarship. C.E.v.d.S. is supported by the European Union's Horizon 2020 research and innovation program Marie Skłodowska-Curie grant (no. 792532). T.M.A. and F.M.-W. are International Society for Advancement of Cytometry Marylou Ingram Scholars. G.H.P. is supported by the Australian Government Research Training Program (RTP) Scholarship. J.A.J. is supported by an NHMRC Early Career Fellowship (no. 1123673). E.B.C. is supported by NHMRC Peter Doherty Fellowship no. 1091516. The Melbourne WHO Collaborating Centre is supported by the Australian Government Department of Health. We acknowledge all DRASTIC (the use of cytokines as a predictor of disease severity in critically ill COVID-patients) investigators from Austin Health and Fiona James, Effie Mouhtouris, and Ana Copaescu for laboratory work and DRASTIC study coordination. The graphical abstract was created with BioRender.com.

AUTHOR CONTRIBUTIONS

K.K. led the study. K.K., T.H.O.N., and A.C.C. supervised the study. K.K., T.H.O.N., M.K., L.C.R., L.H., B.Y.C., C.E.v.d.S., W.Z., and E.B.C. designed the experiments. M.K., L.C.R., L.H., B.Y.C., C.E.v.d.S., J.R.H., W.Z., X.J., L.K., C.Y.W., F.L.M., and T.H.O.N. performed and analyzed the experiments. M.K., T.M.A., G.H.P., F.M.-W., M.N.R., and D.N.E. performed the computational analysis. F.A. and F.K. provided the reagents. J.A.J. and J.A. managed the patient cohorts. J.A.J., N.E.H., C.L.G., O.C.S., J.A.T., C.M.H., J.T.D., S.Y.C.T., D.L.D., T.C.K., A.K.W., S.J.K., J.M., I.T., and A.C.C. recruited the patient cohorts. D.C.J., D.I.G., A.W.C., M.C., N.J.C.K., S.R.L., K.S., T.H.O.N., A.C.C., and K.K. provided intellectual input into the study design and data interpretation. M.K., T.H.O.N., A.C.C., and K.K. wrote the manuscript. All of the authors reviewed and approved the manuscript.

DECLARATION OF INTERESTS

The authors declare no competing interests.

Received: September 17, 2020
Revised: November 5, 2020
Accepted: February 1, 2021
Published: February 5, 2021

REFERENCES

1. Koutsakos, M., and Kedzierska, K. (2020). A race to determine what drives COVID-19 severity. Nature *583*, 366–368.
2. Zhang, X., Tan, Y., Ling, Y., Lu, G., Liu, F., Yi, Z., Jia, X., Wu, M., Shi, B., Xu, S., et al. (2020). Viral and host factors related to the clinical outcome of COVID-19. Nature *583*, 437–440.

3. Thevarajan, I., Nguyen, T.H.O., Koutsakos, M., Druce, J., Caly, L., van de Sandt, C.E., Jia, X., Nicholson, S., Catton, M., Cowie, B., et al. (2020). Breadth of concomitant immune responses prior to patient recovery: a case report of non-severe COVID-19. Nat. Med. *26*, 453–455.

4. Kuri-Cervantes, L., Pampena, M.B., Meng, W., Rosenfeld, A.M., Ittner, C.A.G., Weisman, A.R., Agyekum, R.S., Mathew, D., Baxter, A.E., Vella, L.A., et al. (2020). Comprehensive mapping of immune perturbations associated with severe COVID-19. Sci. Immunol. *5*, eabd7114.

5. Long, Q.X., Tang, X.J., Shi, Q.L., Li, Q., Deng, H.J., Yuan, J., Hu, J.L., Xu, W., Zhang, Y., Lv, F.J., et al. (2020). Clinical and immunological assessment of asymptomatic SARS-CoV-2 infections. Nat. Med. *26*, 1200–1204.

6. Mathew, D., Giles, J.R., Baxter, A.E., Oldridge, D.A., Greenplate, A.R., Wu, J.E., Alanio, C., Kuri-Cervantes, L., Pampena, M.B., D'Andrea, K., et al.; UPenn COVID Processing Unit (2020). Deep immune profiling of COVID-19 patients reveals distinct immunotypes with therapeutic implications. Science *369*, eabc8511.

7. Lucas, C., Wong, P., Klein, J., Castro, T.B.R., Silva, J., Sundaram, M., Ellingson, M.K., Mao, T., Oh, J.E., Israelow, B., et al.; Yale IMPACT Team (2020). Longitudinal analyses reveal immunological misfiring in severe COVID-19. Nature *584*, 463–469.

8. Laing, A.G., Lorenc, A., Del Molino Del Barrio, I., Das, A., Fish, M., Monin, L., Munoz-Ruiz, M., McKenzie, D.R., Hayday, T.S., Francos-Quijorna, I., et al. (2020). A dynamic COVID-19 immune signature includes associations with poor prognosis. Nat. Med. *26*, 1623–1635.

9. Amanat, F., Stadlbauer, D., Strohmeier, S., Nguyen, T.H.O., Chromikova, V., McMahon, M., Jiang, K., Arunkumar, G.A., Jurczyszak, D., Polanco, J., et al. (2020). A serological assay to detect SARS-CoV-2 seroconversion in humans. Nat. Med. *26*, 1033–1036.

10. Grifoni, A., Weiskopf, D., Ramirez, S.I., Mateus, J., Dan, J.M., Moderbacher, C.R., Rawlings, S.A., Sutherland, A., Premkumar, L., Jadi, R.S., et al. (2020). Targets of T Cell Responses to SARS-CoV-2 Coronavirus in Humans with COVID-19 Disease and Unexposed Individuals. Cell *181*, 1489–1501.e15.

11. Juno, J.A., Tan, H.-X., Lee, W.S., Reynaldi, A., Kelly, H.G., Wragg, K., Esterbauer, R., Kent, H.E., Batten, C.J., Mordant, F.L., et al. (2020). Immunogenic profile of SARS-CoV-2 spike in individuals recovered from COVID-19. medRxiv, 2020.2005.2017.20104869.

12. Weiskopf, D., Schmitz, K.S., Raadsen, M.P., Grifoni, A., Okba, N.M.A., Endeman, H., van den Akker, J.P.C., Molenkamp, R., Koopmans, M.P.G., van Gorp, E.C.M., et al. (2020). Phenotype and kinetics of SARS-CoV-2-specific T cells in COVID-19 patients with acute respiratory distress syndrome. Sci. Immunol. *5*, eabd2071.

13. Habel J R, Nguyen, T.H.O., van de Sandt, C.E., Juno, J.A., Chaurasia, P., Wragg, K., Koutsakos, M., Hensen, L., Jia, X., Chua, B., et al. (2020). Suboptimal SARS-CoV-2-specific CD8+ T-cell response associated with the prominent HLA-A*02:01 phenotype. Proc. Natl. Acad. Sci. USA *117*, 24384–24391.

14. Zhou, R., To, K.K., Wong, Y.C., Liu, L., Zhou, B., Li, X., Huang, H., Mo, Y., Luk, T.Y., Lau, T.T., et al. (2020). Acute SARS-CoV-2 Infection Impairs Dendritic Cell and T Cell Responses. Immunity *53*, 864–877.e5.

15. RECOVERY Collaborative Group; Horby, P., Lim, W.S., Emberson, J.R., Mafham, M., Bell, J.L., Linsell, L., Staplin, N., Brightling, C., Ustianowski, A., et al. (2020). Dexamethasone in Hospitalized Patients with Covid-19 - Preliminary Report. N. Engl. J. Med. https://doi.org/10.1056/NEJMoa2021436.

16. Campochiaro, C., and Dagna, L. (2020). The conundrum of interleukin-6 blockade in COVID-19. Lancet Rheumatol. *2*, E579–E580.

17. Dagotto, G., Yu, J., and Barouch, D.H. (2020). Approaches and Challenges in SARS-CoV-2 Vaccine Development. Cell Host Microbe *28*, 364–370.

18. Van Gassen, S., Callebaut, B., Van Helden, M.J., Lambrecht, B.N., Demeester, P., Dhaene, T., and Saeys, Y. (2015). FlowSOM: using self-organizing maps for visualization and interpretation of cytometry data. Cytometry A *87*, 636–645.

19. Putri, G.H., Read, M.N., Irena Koprinska, I., Singh, D., Röhm, U., Ashhurst, T.M., and King, N.J.C. (2019). ChronoClust: Density-based clustering and cluster tracking in high-dimensional time-series data. Knowl. Base. Syst. *174*, 9–26.

20. Moore, J.B., and June, C.H. (2020). Cytokine release syndrome in severe COVID-19. Science *368*, 473–474.

21. Mudd, P.A., Crawford, J.C., Turner, J.S., Souquette, A., Reynolds, D., Bender, D., Bosanquet, J.P., Anand, N.J., Striker, D.A., Martin, R.S., et al. (2020). Targeted Immunosuppression Distinguishes COVID-19 from Influenza in Moderate and Severe Disease. medRxiv.

22. Remy, K.E., Mazer, M., Striker, D.A., Ellebedy, A.H., Walton, A.H., Unsinger, J., Blood, T.M., Mudd, P.A., Yi, D.J., Mannion, D.A., et al. (2020). Severe immunosuppression and not a cytokine storm characterizes COVID-19 infections. JCI Insight *5*, 140329.

23. Sinha, P., Matthay, M.A., and Calfee, C.S. (2020). Is a "Cytokine Storm" Relevant to COVID-19? JAMA Intern. Med. *180*, 1152–1154.

24. Koutsakos, M., Illing, P.T., Nguyen, T.H.O., Mifsud, N.A., Crawford, J.C., Rizzetto, S., Eltahla, A.A., Clemens, E.B., Sant, S., Chua, B.Y., et al. (2019). Human $CD8^+$ T cell cross-reactivity across influenza A, B and C viruses. Nat. Immunol. *20*, 613–625.

25. Koutsakos, M., Wheatley, A.K., Loh, L., Clemens, E.B., Sant, S., Nüssing, S., Fox, A., Chung, A.W., Laurie, K.L., Hurt, A.C., et al. (2018). Circulating T_{FH} cells, serological memory, and tissue compartmentalization shape human influenza-specific B cell immunity. Sci. Transl. Med. *10*, eaan8405.

26. Wang, Z., Zhu, L., Nguyen, T.H.O., Wan, Y., Sant, S., Quiñones-Parra, S.M., Crawford, J.C., Eltahla, A.A., Rizzetto, S., Bull, R.A., et al. (2018). Clonally diverse $CD38^+HLA\text{-}DR^+CD8^+$ T cells persist during fatal H7N9 disease. Nat. Commun. *9*, 824.

27. Wong, S.S., Oshansky, C.M., Guo, X.J., Ralston, J., Wood, T., Seeds, R., Newbern, C., Waite, B., Reynolds, G., Widdowson, M.A., et al.; SHIVERS Investigation Team (2018). Severe Influenza Is Characterized by Prolonged Immune Activation: Results From the SHIVERS Cohort Study. J. Infect. Dis. *217*, 245–256.

28. Koutsakos, M., Nguyen, T.H.O., and Kedzierska, K. (2019). With a Little Help from T Follicular Helper Friends: Humoral Immunity to Influenza Vaccination. J. Immunol. *202*, 360–367.

29. Teachey, D.T., Lacey, S.F., Shaw, P.A., Melenhorst, J.J., Maude, S.L., Frey, N., Pequignot, E., Gonzalez, V.E., Chen, F., Finklestein, J., et al. (2016). Identification of Predictive Biomarkers for Cytokine Release Syndrome after Chimeric Antigen Receptor T-cell Therapy for Acute Lymphoblastic Leukemia. Cancer Discov. *6*, 664–679.

30. Oshansky, C.M., Gartland, A.J., Wong, S.S., Jeevan, T., Wang, D., Roddam, P.L., Caniza, M.A., Hertz, T., Devincenzo, J.P., Webby, R.J., and Thomas, P.G. (2014). Mucosal immune responses predict clinical outcomes during influenza infection independently of age and viral load. Am. J. Respir. Crit. Care Med. *189*, 449–462.

31. Wang, Z., Zhang, A., Wan, Y., Liu, X., Qiu, C., Xi, X., Ren, Y., Wang, J., Dong, Y., Bao, M., et al. (2014). Early hypercytokinemia is associated with interferon-induced transmembrane protein-3 dysfunction and predictive of fatal H7N9 infection. Proc. Natl. Acad. Sci. USA *111*, 769–774.

32. Jozwik, A., Habibi, M.S., Paras, A., Zhu, J., Guvenel, A., Dhariwal, J., Almond, M., Wong, E.H.C., Sykes, A., Maybeno, M., et al. (2015). RSV-specific airway resident memory CD8+ T cells and differential disease severity after experimental human infection. Nat. Commun. *6*, 10224.

33. Huber, J.E., Ahlfeld, J., Scheck, M.K., Zaucha, M., Witter, K., Lehmann, L., Karimzadeh, H., Pritsch, M., Hoelscher, M., von Sonnenburg, F., et al. (2020). Dynamic changes in circulating T follicular helper cell composition predict neutralising antibody responses after yellow fever vaccination. Clin. Transl. Immunology *9*, e1129.

34. Zhang, J., Liu, W., Wen, B., Xie, T., Tang, P., Hu, Y., Huang, L., Jin, K., Zhang, P., Liu, Z., et al. (2019). Circulating $CXCR3^+$ Tfh cells positively correlate with neutralizing antibody responses in HCV-infected patients. Sci. Rep. *9*, 10090.

35. Kaneko, N., Kuo, H.H., Boucau, J., Farmer, J.R., Allard-Chamard, H., Mahajan, V.S., Piechocka-Trocha, A., Lefteri, K., Osborn, M., Bals, J., et al.; Massachusetts Consortium on Pathogen Readiness Specimen Working Group (2020). Loss of Bcl-6-Expressing T Follicular Helper Cells and Germinal Centers in COVID-19. Cell *183*, 143–157.e13.

36. Hill, D.L., Pierson, W., Bolland, D.J., Mkindi, C., Carr, E.J., Wang, J., Houard, S., Wingett, S.W., Audran, R., Wallin, E.F., et al. (2019). The adjuvant GLA-SE promotes human Tfh cell expansion and emergence of public TCRβ clonotypes. J. Exp. Med. *216*, 1857–1873.

37. Liang, F., Lindgren, G., Sandgren, K.J., Thompson, E.A., Francica, J.R., Seubert, A., De Gregorio, E., Barnett, S., O'Hagan, D.T., Sullivan, N.J., et al. (2017). Vaccine priming is restricted to draining lymph nodes and controlled by adjuvant-mediated antigen uptake. Sci. Transl. Med. *9*, eaal2094.

38. Mastelic Gavillet, B., Eberhardt, C.S., Auderset, F., Castellino, F., Seubert, A., Tregoning, J.S., Lambert, P.H., de Gregorio, E., Del Giudice, G., and Siegrist, C.A. (2015). MF59 Mediates Its B Cell Adjuvanticity by Promoting T Follicular Helper Cells and Thus Germinal Center Responses in Adult and Early Life. J. Immunol. *194*, 4836–4845.

39. Thanh Le, T., Andreadakis, Z., Kumar, A., Gómez Román, R., Tollefsen, S., Saville, M., and Mayhew, S. (2020). The COVID-19 vaccine development landscape. Nat. Rev. Drug Discov. *19*, 305–306.

40. Roche. Roche provides an update on the phase III COVACTA trial of Actemra/RoActemra in hospitalised patients with severe COVID-19 associated pneumonia.https://www.roche.com/investors/updates/inv-update-2020-07-29.htm.

41. Sanofi. Sanofi and Regeneron provide update on Kevzara® (sarilumab) Phase 3 U.S. trial in COVID-19 patients.https://www.sanofi.com/en/media-room/press-releases/2020/2020-07-02-22-30-00.

42. Rose-John, S. (2018). Interleukin-6 Family Cytokines. Cold Spring Harb. Perspect. Biol. *10*, a028415.

43. Wilson, J.G., Simpson, L.J., Ferreira, A.M., Rustagi, A., Roque, J., Asuni, A., Ranganath, T., Grant, P.M., Subramanian, A., Rosenberg-Hasson, Y., et al. (2020). Cytokine profile in plasma of severe COVID-19 does not differ from ARDS and sepsis. JCI Insight *5*, e140289.

44. Kimmig, L.M., Wu, D., Gold, M., Pettit, N.N., Pitrak, D., Mueller, J., Husain, A.N., Mutlu, E.A., and Mutlu, G.M. (2020). IL6 inhibition in critically ill COVID-19 patients is associated with increased secondary infections. Front. Med. *7*, 583897.

45. Briso, E.M., Dienz, O., and Rincon, M. (2008). Cutting edge: soluble IL-6R is produced by IL-6R ectodomain shedding in activated CD4 T cells. J. Immunol. *180*, 7102–7106.

46. Cox, M.A., Kahan, S.M., and Zajac, A.J. (2013). Anti-viral CD8 T cells and the cytokines that they love. Virology *435*, 157–169.

47. Nakanishi, K. (2018). Unique Action of Interleukin-18 on T Cells and Other Immune Cells. Front. Immunol. *9*, 763.

48. Tsai, C.Y., Liong, K.H., Gunalan, M.G., Li, N., Lim, D.S., Fisher, D.A., MacAry, P.A., Leo, Y.S., Wong, S.C., Puan, K.J., and Wong, S.B. (2015). Type I IFNs and IL-18 regulate the antiviral response of primary human γδ T cells against dendritic cells infected with Dengue virus. J. Immunol. *194*, 3890–3900.

49. McKie, E.A., Reid, J.L., Mistry, P.C., DeWall, S.L., Abberley, L., Ambery, P.D., and Gil-Extremera, B. (2016). A Study to Investigate the Efficacy and Safety of an Anti-Interleukin-18 Monoclonal Antibody in the Treatment of Type 2 Diabetes Mellitus. PLoS ONE *11*, e0150018.

50. Yasuda, K., Nakanishi, K., and Tsutsui, H. (2019). Interleukin-18 in Health and Disease. Int. J. Mol. Sci. *20*, 649.

51. Ndhlovu, Z.M., Kamya, P., Mewalal, N., Kløverpris, H.N., Nkosi, T., Pretorius, K., Laher, F., Ogunshola, F., Chopera, D., Shekhar, K., et al. (2015). Magnitude and Kinetics of CD8+ T Cell Activation during Hyperacute HIV Infection Impact Viral Set Point. Immunity *43*, 591–604.

52. Ruibal, P., Oestereich, L., Lüdtke, A., Becker-Ziaja, B., Wozniak, D.M., Kerber, R., Korva, M., Cabeza-Cabrerizo, M., Bore, J.A., Koundouno, F.R., et al. (2016). Unique human immune signature of Ebola virus disease in Guinea. Nature *533*, 100–104.

53. Zubkova, I., Duan, H., Wells, F., Mostowski, H., Chang, E., Pirollo, K., Krawczynski, K., Lanford, R., and Major, M. (2014). Hepatitis C virus clearance correlates with HLA-DR expression on proliferating CD8+ T cells in immune-primed chimpanzees. Hepatology *59*, 803–813.

54. Chandele, A., Sewatanon, J., Gunisetty, S., Singla, M., Onlamoon, N., Akondy, R.S., Kissick, H.T., Nayak, K., Reddy, E.S., Kalam, H., et al. (2016). Characterization of Human CD8 T Cell Responses in Dengue Virus-Infected Patients from India. J. Virol. *90*, 11259–11278.

55. Glaría, E., and Valledor, A.F. (2020). Roles of CD38 in the Immune Response to Infection. Cells *9*, E228.

56. Caly, L., Druce, J., Roberts, J., Bond, K., Tran, T., Kostecki, R., Yoga, Y., Naughton, W., Taiaroa, G., Seemann, T., et al. (2020). Isolation and rapid sharing of the 2019 novel coronavirus (SARS-CoV-2) from the first patient diagnosed with COVID-19 in Australia. Med. J. Aust. *212*, 459–462.

57. Juno, J.A., Tan, H.X., Lee, W.S., Reynaldi, A., Kelly, H.G., Wragg, K., Esterbauer, R., Kent, H.E., Batten, C.J., Mordant, F.L., et al. (2020). Humoral and circulating follicular helper T cell responses in recovered patients with COVID-19. Nat. Med. *26*, 1428–1434.

58. Ashhurst, T.M., Cox, D.A., Smith, A.L., and King, N.J.C. (2019). Analysis of the Murine Bone Marrow Hematopoietic System Using Mass and Flow Cytometry. Methods Mol. Biol. *1989*, 159–192.

59. Wickham, H. (2016). ggplot2: Elegant Graphics for Data Analysis (Springer-Verlag).

60. Gu, Z., Gu, L., Eils, R., Schlesner, M., and Brors, B. (2014). circlize implements and enhances circular visualization in R. Bioinformatics *30*, 2811–2812.

61. Sachs, M.C. (2017). plotROC: A Tool for Plotting ROC Curves. J. Stat. Softw. *79*, 0.18637/jss.v079.c02.

62. Van Gassen, S., Gaudilliere, B., Angst, M.S., Saeys, Y., and Aghaeepour, N. (2020). CytoNorm: A Normalization Algorithm for Cytometry Data. Cytometry A *97*, 268–278.

63. McInnes, L., and Healy, J. (2018). UMAP: Uniform Manifold Approximation and Projection for Dimension Reduction. arXiv, 1802.03426v3. http://arxiv.org/abs/03426v3.

64. Roederer, M., Nozzi, J.L., and Nason, M.C. (2011). SPICE: exploration and analysis of post-cytometric complex multivariate datasets. Cytometry A *79*, 167–174.

65. Stadlbauer, D., Amanat, F., Chromikova, V., Jiang, K., Strohmeier, S., Arunkumar, G.A., Tan, J., Bhavsar, D., Capuano, C., Kirkpatrick, E., et al. (2020). SARS-CoV-2 Seroconversion in Humans: A Detailed Protocol for a Serological Assay, Antigen Production, and Test Setup. Curr. Protoc. Microbiol. *57*, e100.

STAR★METHODS

KEY RESOURCES TABLE

REAGENT or RESOURCE	SOURCE	IDENTIFIER
Antibodies		
CD45RA HI100 FITC	BD PharMingen	Cat#555488; RRID: AB_395879
CD8a SK1 PerCP-Cy5.5	BD PharMingen	Cat#565310; RRID: AB_2687497
CD56 MEM-188 APC	Biolegend	Cat#304610; RRID: AB_314452
CD16 3G8 AF700	Biolegend	Cat#302026; RRID: AB_2278418
CD14 MΦP9 APC-Cy7	BD PharMingen	Cat#560180; RRID: AB_1645464
CD19 HIB19 BV570	Biolegend	Cat#302236; RRID: AB_2563606
HLA-DR L243 BV605	Biolegend	Cat#307640; RRID: AB_2561913
CD4 SK3 BV650	BD Biosciences	Cat#563875; RRID: AB_2744425
CD27 L128 BV711	BD Horizon	Cat#563167; RRID: AB_2738042
CD38 HIT2 BV786	BD Horizon	Cat#563964; RRID: AB_2738515
CD3 UCHT1 PECF594	BD Biosciences	Cat#562280; RRID: AB_11153674
CD45RA HI100 FITC	BD PharMingen	Cat#555488; RRID: AB_395879
CD8a RPA-T8 BV421	Biolegend	Cat#301036; RRID: AB_10960142
CD14 MΦP9 APC-H7	BD PharMingen	Cat#560180; RRID: AB_1645464
CD19 SJ25C1 APC-H7	Biolegend	Cat#560177; RRID: AB_1645470
HLA-DR L243 BV605	Biolegend	Cat#307640; RRID: AB_2561913
CD4 SK3 BV650	BD Biosciences	Cat#563875; RRID: AB_2744425
CD27 L128 BV711	BD Horizon	Cat#563167; RRID: AB_2738042
CD38 HIT2 BV786	BD Horizon	Cat#563964; RRID: AB_2738515
CD3 UCHT1 PECF594	BD Biosciences	Cat#562280; RRID: AB_11153674
Granzyme A CB9 PE	eBioscience	Cat#12-9177-42; RRID: AB_2572701
Granzyme B GB11 AF700	BD PharMingen	Cat#560213; RRID: AB_1645453
Granzyme K G3H69 PerCP-eFluor710	eBioscience	Cat#46-8897-42; RRID: AB_2573854
Granzyme M 4B2G4 eFluor660	eBioscience	Cat#50-9774-42; RRID: AB_2574374
Perforin B-D48 Pe-Cy7	Biolegend	Cat#353316; RRID: AB_2571973
Peroxidase AffiniPure goat anti-human IgG, Fcγ fragment specific	Jackson ImmunoResearch	Cat#109-035-098; RRID: AB_2337586
Rat anti-human IgA mAb MT20, alkaline phosphate-conjugated	MabTech	Cat#3860-9A; RRID: AB_10736550
Mouse anti-human IgM mAb MT22, biotinylated	MabTech	Cat#3880-6-250
Bacterial and virus strains		
SARS-CoV-2 isolate CoV/Australia/VIC01/2020	Caly et al.[56]	N/A
Biological samples		
Blood samples (peripheral blood mononuclear cells (PBMCs), serum and plasma samples) from COVID-19 patients and healthy control individuals	Alfred Hospital, Melbourne Health, Monash Health, Austin Health, The University of Melbourne and James Cook University (Australia)	N/A
Chemicals, peptides, and recombinant proteins		
AccuCheck Counting Beads	Thermo Fisher Scientific	Cat#PCB100
3,3′,5,5′-Tetramethylbenzidine (TMB) Liquid Substrate System for ELISA, peroxidase substrate	Sigma	Cat#T0440-1L

(*Continued on next page*)

Continued

REAGENT or RESOURCE	SOURCE	IDENTIFIER
Alkaline phosphatase yellow (pNPP) liquid substrate for ELISA	Sigma	Cat#P7998-100ML
Pierce High Sensitivity Streptavidin-HRP	Thermo Fisher Scientific	Cat#21130
SARS-CoV-2 RBD protein	Amanat et al.[9]	N/A
SARS-CoV-2 Spike protein	Juno et al.[57]	N/A
Critical commercial assays		
eBioscience™ Foxp3/Transcription Factor Staining Buffer Set	Thermo Fisher Scientific	Cat#00-5521-00
LEGENDplex Human Inflammation Panel 1 kit	BioLegend	Cat#740809
Human IL-6R alpha DuoSet ELISA kit	R&D Systems	Cat#RDSDY227
Experimental models: cell lines		
Vero C1008, African Green monkey kidney cells	ATCC	Cat#CRL-1586; Lot#3338237; RRID: CVCL_0574
Software and algorithms		
R v3.6.2	The Comprehensive R Archive Network	https://cran.r-project.org
Spectre R package	Ashhurst et al.[58]	https://github.com/ImmuneDynamics/Spectre
ggplot2 R package	Wickham[59]	https://cran.r-project.org/web/packages/ggplot2/index.html
circlize R package	Gu et al.[60]	https://cran.r-project.org/web/packages/circlize/index.html
corrplot R package	N/A	https://cran.r-project.org/web/packages/corrplot/index.html
pROC R package	Sachs[61]	https://cran.r-project.org/web/packages/pROC/index.html
plotROC package	Sachs [61]	https://cran.r-project.org/web/packages/plotROC/index.html
FlowJo v10.5.3	N/A	https://www.flowjo.com
CytoNorm	Van Gassen et al.[62]	https://www.github.com/saeyslab/CytoNorm
FlowSOM	Van Gassen et al.[18]	https://github.com/SofieVG/FlowSOM
UMAP	McInnes and Healy[63]	https://arxiv.org/abs/1802.03426
TrackSOM	This paper	https://www.github.com/ghar1821/TrackSOM
Pestle v2 and Spice v6	Roederer et al.[64]	https://niaid.github.io/spice/
Prism v8.3.1	GraphPad	https://www.graphpad.com
BD FACS Diva v8.0.1	BD Biosciences	https://www.bdbiosciences.com/en-us/instruments/research-instruments/research-software/flow-cytometry-acquisition/facsdiva-software

RESOURCE AVAILABILITY

Lead contact

Further information and requests for resources and reagents should be directed to and will be fulfilled by the Lead Contact, Katherine Kedzierska (kkedz@unimelb.edu.au).

Materials availability

This study did not generate new unique reagents.

Data and code availability

Data supporting the findings of this study are available without restriction from the Lead Contact, Katherine Kedzierska (kkedz@unimelb.edu.au) upon request. αcode can be downloaded from https://www.github.com/ghar1821/TrackSOM.

EXPERIMENTAL MODEL AND SUBJECT DETAILS

We enrolled consenting adult patients at Victorian hospitals during the first and second waves of the SARS-CoV-2 pandemic (February-September 2020) with influenza-like illness (ILI), including 33 SARS-CoV-2 PCR-positive patients and 11 patients who presented with ILI but were SARS-CoV-2 PCR negative as negative serological controls. Out of the 33 COVID-19 symptomatic/hospitalized patients, 20 were admitted to the ward, with 4 patients requiring non-invasive oxygen support, 12 were in ICU with 8 requiring mechanical ventilation and 3 requiring non-invasive oxygen support, and 1 was an outpatient (Table S1). For 7 ICU patients only plasma samples were available for cytokine analysis. No patients died during the study. Heparinised blood samples were collected within 24-72 hours of hospital admission (Acute Visit 1, A1) with sequential bleeds every 1-5 days apart until discharge (A2-A6). For 12 COVID-19 patients, a follow-up blood sample was taken approximately 30 days after discharge/recovery (Convalescent Visit 1, C1; median 43 days, 31-80 range). Additional SARS-CoV-2 PCR-confirmed patients (n = 52) and pre-pandemic healthy donors (n = 66) were recruited through contacts with the investigators and asked to provide a blood sample at the time of enrolment (A1 n = 1 and C1 n = 51; median 40 days, 26-102 range) and an additional time-point where available (C2). Demographic, clinical and sampling information for COVID-19 patients are described in Table S2.

Human experimental work was conducted according to the Declaration of Helsinki Principles and the Australian National Health and Medical Research Council Code of Practice. All participants provided written informed consent prior to the study. The study was approved by the Alfred Hospital (#280/14), Melbourne Health (HREC/17/MH/53), Monash Health (HREC/15/MonH/64/2016.196), Austin Health (HREC/63201/Austin-2020), The University of Melbourne (#2056689, #2056761, #1442952, #1955465, #2057366.1 and #1443389) and James Cook University (H7886) Human Research Ethics Committees.

METHOD DETAILS

Whole blood flow cytometry

Fresh whole blood was used to measure cell populations, essentially as described,[3] using three human antibody panels for enumerating immune cell activation (monocytes and T/B/NK/γδ cells), T_{FH} and ASC cell activation, and cytotoxicity profiles of T cell's expressing intracellular granzymes (A, B, K and M) and perforin. Cells were stained, RBC lysed, then fixed in 1% PFA, or intracellularly stained using the eBioscience™ Foxp3/Transcription Factor Staining Buffer Set (Thermo Fisher Scientific, Carlsbad, CA, USA), as previously described.[3] AccuCheck Counting Beads (Thermo Fisher Scientific) were added to the immune cell activation panel for calculating absolute numbers just prior to acquisition. Samples were acquired on a BD LSRII Fortessa and analyzed using FlowJo v10 software.

RBD and Spike protein ELISAs

Detection of RBD- and Spike-specific antibodies was performed as described[9,65] with the following modifications; Nunc MaxiSorp flat bottom 96-well plates (Thermo Fisher Scientific) were used for antigen coating, blocking performed with PBS (containing w/v 10% BSA) and serial dilutions performed in PBS (containing v/v 0.05% Tween and w/v 5% BSA). For detection of IgG and IgA, peroxidase-conjugated goat anti-human IgG (Fcγ fragment specific; Jackson ImmunoResearch) or alkaline phosphate-conjugated rat anti-human IgA (mAb MT20; MabTech), was used and developed with TMB (Sigma) substrate for IgG or pNPP (Sigma) for IgA. For IgM, biotinylated mAb MT22 and peroxidase-conjugated streptavidin (Pierce; Thermo Fisher Scientific) was used. Peroxidase reactions were stopped using 1M H_3PO_4 and plates read on a Multiskan plate reader (Labsystems). Inter- and intra-experimental measurements were normalized using a positive control plasma from a COVID-19 patient (#1-073) run on each plate. Endpoint titers were determined by interpolation from a sigmodial curve fit (all R-squared values > 0.95; GraphPad Prism 8) as the reciprocal dilution of plasma that produced $\geq$ 15% (for IgA and IgG) or $\geq$ 30% (for IgM) absorbance of the positive control at a 1:31.6 (IgG and IgM) or 1:10 dilution (IgA). Patients were considered to have seroconverted if titers were above the mean of titers from 16 healthy non-COVID19 donors +2× the standard deviation.

Antibody avidity assay

The avidity of RBD-specific IgG and IgM antibodies in plasma samples was measured using urea as the chaotropic agent. Following incubation of plasma at a 1:31.6, 1:100 and 1:316 dilution on antigen-coated plates for 2 h, 6M of urea was added after washing and incubated for 15 min. Bound antibodies were then detected using respective secondary detection reagents in procedures described above. Antibody avidity is expressed as the percentage of remaining antibody bound to antigen following urea treatment compared to the absence of urea. Data of 1:100 diluted plasma for IgG and 1:316 for IgM are reported in Figure 4E, with the rest of the data presented in Figure S7A. Data from 1:100 and 1:316 diluted plasma were used for linear regression analysis of IgG and IgM avidity respectively in Figure 4F.

Microneutralisation assay

Microneutralisation activity of serum samples was assessed as previously described.[57] SARS-CoV-2 isolate CoV/Australia/VIC01/2020[56] was propagated in Vero cells and stored at −80°C. Serum samples were heat inactivated at 56°C for 30 min. Samples were serially diluted two-fold starting at 1:20 and 100 $TCID_{50}$ of SARS-CoV-2 in MEM/0.5% BSA were added and incubated at room temperature for 1 h. Residual virus infectivity in the serum/virus mixtures was assessed in quadruplicate wells of Vero cells incubated in serum-free media containing 1 μg ml−1 of TPCK trypsin at 37°C and 5% CO2; viral cytopathic effect was read on day 5. The neutralising antibody titer was calculated using the Reed–Muench method, as previously described.[57]

Cytokine analysis

Patient's plasma was diluted 1:2 for measuring IL-1β, IFN-α2, IFNγ, TNFα, MCP-1 (CCL2), IL-6, IL-8 (CXCL8), IL-10, IL-12p70, IL-17A, IL-18, IL-23 and IL-33 using the LEGENDplex Human Inflammation Panel 1 kit, according to manufacturer's instructions (BioLegend, San Diego, CA, USA). sIL-6R levels were measured in plasma (diluted 1:300) using the Human IL-6R alpha DuoSet ELISA kit (R&D Systems, Minneapolis, MN, USA) according to manufacturer's instructions.

QUANTIFICATION AND STATISTICAL ANALYSIS

Computational flow cytometry analysis

Computational analysis of data was performed using the Spectre R package[58] (https://github.com/ImmuneDynamics/Spectre). Samples were initially prepared in FlowJo, and populations of interest were exported as CSV files containing scale value (raw) data. In R, data were subject to arcsinh transformation, and data below the limit of detection were compressed to reduce the contribution of noise to the clustering process. Batch alignment was then performed using CytoNorm[62] as implemented in Spectre. Aligned data were then clustered using FlowSOM and a subset of cells plotted using UMAP.[63] Cluster identities were annotated manually. Cellular expression of dynamic markers (CD38, HLA-DR, ICOS, PD-1, granzymes, or perforin) was determined on each population using the non-aligned arcsinh transformed data, and adjusted manually per sample where required. Data from the immune panel were clustered and plotted by UMAP using forward scatter (FSC), side scatter (SSC), CD16, CD14, CD56, CD19, TCRγδ, CD3, CD4, CD8, CD45RA, CD27, CD38, and HLA-DR. Immune cell lineages were manually annotated based on marker expression: eosinophils ($FSC^{hi}SSC^{hi}CD16^{-}$), neutrophils ($FSC^{int}SSC^{int}CD16^{hi}$), monocytes ($FSC^{int}CD14^{+}$), B cells ($CD19^{+}$), NK cells ($CD56^{+}$), gamma-delta T cells ($TCRgd^{+}CD3^{+}$), $CD4^{+}$ T cells ($CD3^{+}CD4^{+}$), and $CD8^{+}$ T cells ($CD3^{+}CD8^{+}$). Subsequently, population subsets were manually annotated based on marker expression: monocytes (classical $CD14^{+}CD16^{-}$ and non-classical $CD14^{-}CD16^{+}$), B cells (naive $CD27^{-}CD38^{-}$, memory $CD27^{+}CD38^{-}$, ASC $CD27^{+}CD38^{+}$), NK cells ($CD56^{bri}$ and $CD56^{dim}$), $CD4^{+}$ T cells (naive $CD45RA^{+}CD27^{+}$, T_{EMRA} $CD45RA^{+}CD27^{-}$, T_{CM} $CD45RA^{-}CD27^{+}$, and T_{EM} $CD45RA^{-}CD27^{-}$), and $CD8^{+}$ T cells (naive $CD45RA^{+}CD27^{+}$, T_{EMRA} $CD45RA^{+}CD27^{-}$, T_{CM} $CD45RA^{-}CD27^{+}$, and T_{EM} $CD45RA^{-}CD27^{-}$). Lymphocytes from the T_{FH} & B cell panel were clustered and plotted by UMAP using on CD45, CD3, CD19, CD4, CD8, CXCR5, CXCR3, CD27, CD38. $CD4^{+}$ T cell subsets were manually annotated based on marker expression: T_H1 cells ($CXCR5^{-}CXCR3^{+}$), $T_H2/17$ cells ($CXCR5^{-}CXCR3^{-}$), $T_{FH}1$ cells ($CXCR5^{+}CXCR3^{+}$), and $T_{FH}2/17$ cells ($CXCR5^{+}CXCR3^{-}$). $CD3^{+}$ cells from the cytotoxicity panel were clustered and plotted by UMAP using CD4, CD8, CD45RA, CD27. $CD4^{+}$ and $CD8^{+}$ T cell populations were defined as above for naive $CD45RA^{+}CD27^{+}$, T_{EMRA} $CD45RA^{+}CD27^{-}$, T_{CM} $CD45RA^{-}CD27^{+}$, and T_{EM} $CD45RA^{-}CD27^{-}$.

Summary statistics, scatter graphs, volcano plots and PCA plots were created in R, where comparisons were performed using a Wilcoxon rank-sum test (equivalent to the Mann-Whitney test) with the *wilcox.test* function in R. Statistics displayed in scatter graphs were uncorrected, and statistics displayed in volcano plots were corrected with a False Discovery Rate (FDR) adjustment. TrackSOM is a time series-based clustering and cluster evolution tracking algorithm which that combines FlowSOM's single time-point clustering capacity with ChronoClust's[19] tracking of cluster developments over time. TrackSOM was performed on the first immunophenotyping panel by initially clustering data from all time points using FlowSOM, and thereafter tracking the resulting metaclusters and clusters using ChronoClust's tracking mechanism. TrackSOM was using 10x10 grid, producing 40 metaclusters per time. Binned groups are outlined in Table S3.

Statistical analyses

Statistical significance was assessed using Mann-Whitney, Wilcoxon signed-rank test or Kruskal-Wallis test with Dunn's correction for multiple comparisons in Prism 8 (GraphPad) unless stated otherwise. Analysis of immune parameters against days post-onset were visualized in R 3.6.2 using the ggplot2 package[59] using LOESS fitting with 95% confidence intervals shaded in gray. Correlations were assessed using Spearman's correlation coefficient (r_s) and visualized in R 3.6.2 as circos plots using the circlize package[60] or heatmaps using the corrplot package and p values of correlations were corrected for multiple comparisons by FDR in R 3.6.2. Cytokine concentrations were $\log_{10}(x+1)$ transformed for correlation analysis. Linear regression analysis was performed in Prism 8 (GraphPad). AUROC analysis was performed in R 3.6.2 using the pROC and plotROC packages.[61] Pie charts in Figure 3 were generated using Pestle v2 and Spice v6 software[64] and *p-value*s were calculated using a Permutation Test. *P*-values lower than 0.05 were considered statistically significant.